iScience

Article

Basic Fibroblast Growth Factor 2-Induced Proteome Changes Endorse Lewy Body Pathology in Hippocampal Neurons

promotes

basic fibroblast growth factor

reshapes expression of

exosome release

Lewy body associate proteins in hippocampal neurons and exosomes

endorses Lewy body pathology

to neighboring brain regions and cells

via exosome mediated transfer

Rohit Kumar,
Sainitin
Donakonda,
Stephan A. Müller,
Stefan F.
Lichtenthaler, Kai
Bötzel, Günter U.
Höglinger,
Thomas
Koeglsperger

rohit.kumar@dzne.de (R.K.)
thomas.koeglsperger@dzne.
de (T.K.)

HIGHLIGHTS

bFGF enhances the neuronal release or extracellular vesicles (EVs)

bFGF induces proteomic changes in the neuronal cell lysate and in neuronal EVs

bFGF incites changes in Lewy body pathology (LBP)-linked protein networks

bFGF-induced molecular interactions may endorse LBP
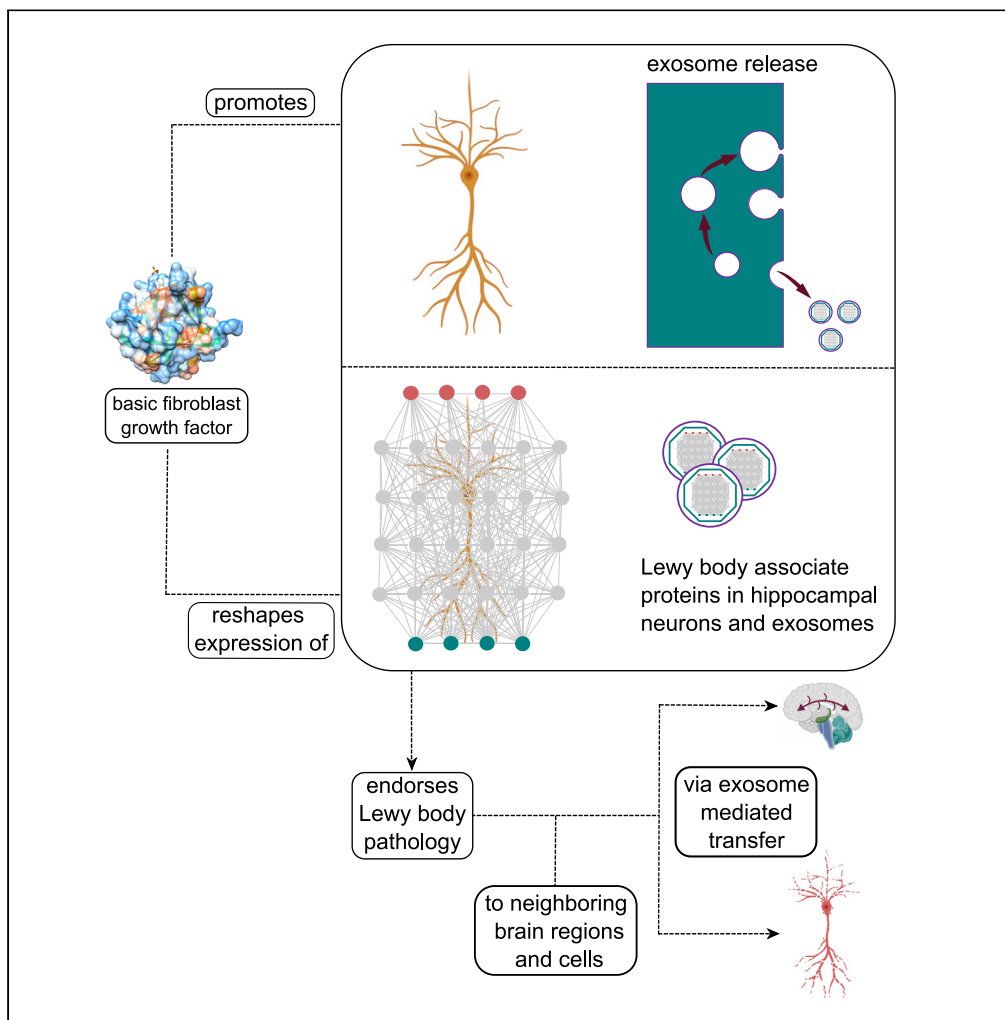
iScience

Article

Basic Fibroblast Growth Factor 2-Induced Proteome Changes Endorse Lewy Body Pathology in Hippocampal Neurons

Rohit Kumar,[1,2,3,8,*] Sainitin Donakonda,[4,8] Stephan A. Müller,[1] Stefan F. Lichtenthaler,[1,6,7] Kai Bötzel,[3] Günter U. Höglinger,[1,2,5] and Thomas Koeglsperger[1,3,9,*]

SUMMARY

Hippocampal Lewy body pathology (LBP) is associated with changes in neurotrophic factor signaling and neuronal energy metabolism. LBP progression is attributed to the aggregation of α-synuclein (α-Syn) and its cell-to-cell transmission via extracellular vehicles (EVs). We recently discovered an enhanced EV release in basic fibroblast growth factor (bFGF)-treated hippocampal neurons. Here, we examined the EV and cell lysate proteome changes in bFGF-treated hippocampal neurons. We identified n = 2,310 differentially expressed proteins (DEPs) induced by bFGF. We applied weighted protein co-expression network analysis (WPCNA) to generate protein modules from DEPs and mapped them to published LBP datasets. This approach revealed n = 532 LBP-linked DEPs comprising key α-Syn-interacting proteins, LBP-associated RNA-binding proteins (RBPs), and neuronal ion channels and receptors that can impact LBP onset and progression. In summary, our deep proteomic analysis affirms the potential influence of bFGF signaling on LBP-related proteome changes and associated molecular interactions.

INTRODUCTION

Synucleinopathies are characterized by the gradual appearance of intraneuronal inclusion bodies, termed Lewy bodies (LBs). These conditions encompass Parkinson's disease (PD) as well as PD dementia (PDD) and dementia with Lewy bodies (DLB) (Galasko, 2017). The latter two entities are characterized by the presence of LBs in hippocampal neurons and associated memory circuits (McKeith et al., 2017). In accord with such a distribution, cognitive deficits including impaired learning and memory are important clinical features of PDD and DLBs. LBs are intraneuronal protein aggregates composed of crowded organelles and lipid membranes and the protein alpha-synuclein (α-Syn) (Shahmoradian et al., 2019; Spillantini et al., 1997). The exact mechanism of α-Syn-induced neuronal dysfunction and death remains elusive, but prior research implicated changes in neurotrophic factor signaling and neuronal energy metabolism during pathological changes. In addition, cell-to-cell transmission of α-Syn through extracellular vehicles (EVs) likely contributes to the spread of pathology in these conditions. The molecular factors that control neuronal EV release are therefore likely to contribute to LB progression.

FGFs are a family of pleiotropic growth and differentiation factors that regulate CNS homeostasis in health and disease. Although FGFs are best known for their roles in the early steps of patterning the neural primordium and proliferation of neural progenitors, they have equally important roles in the adult brain, where they regulate neuronal calcium homeostasis and plasticity further promoting neuroprotection and repair in response to neural tissue damage. In addition to these physiological roles, basic fibroblast growth factor (bFGF) has been linked with responses to neuronal injury (Fagel et al., 2009; Timmer et al., 2004; Yoshimura et al., 2001; Guillemot and Zimmer, 2011) or to psychiatric conditions (Turner et al., 2012; Deng et al., 2019). In addition to these well-known roles of bFGF, we have recently demonstrated bFGF-controlled release of EVs from hippocampal neurons (Kumar et al., 2020a). Because of these functions, bFGF may likewise affect LB-associated pathological changes.

Here, we investigated the cell lysate (CL) and EV proteome changes of hippocampal neurons in response to bFGF. Using high-resolution mass spectrometry (MS), we quantified differentially expressed proteins (DEPs) in the CL and EV fractions of bFGF-treated hippocampal neurons. To capture the protein

[1]German Center for Neurodegenerative Diseases (DZNE), 81337 Munich, Germany

[2]Faculty of Medicine, Klinikum rechts der Isar, Technical University of Munich, 81675 Munich, Germany

[3]Department of Neurology, Ludwig Maximilian University, 81377 Munich, Germany

[4]Institute of Immunology and Experimental Oncology, Technical University of Munich, 81675 Munich, Germany

[5]Department of Neurology, Hannover Medical School (MHH), 30625 Hannover, Germany

[6]Neuroproteomics, School of Medicine, Klinikum rechts der Isar, Technical University of Munich, 81675 Munich, Germany

[7]Munich Cluster for Systems Neurology (SyNergy), 81377 Munich, Germany

[8]These authors contributed equally

[9]Lead Contact

*Correspondence:
rohit.kumar@dzne.de (R.K.),
thomas.koeglsperger@dzne.de (T.K.)
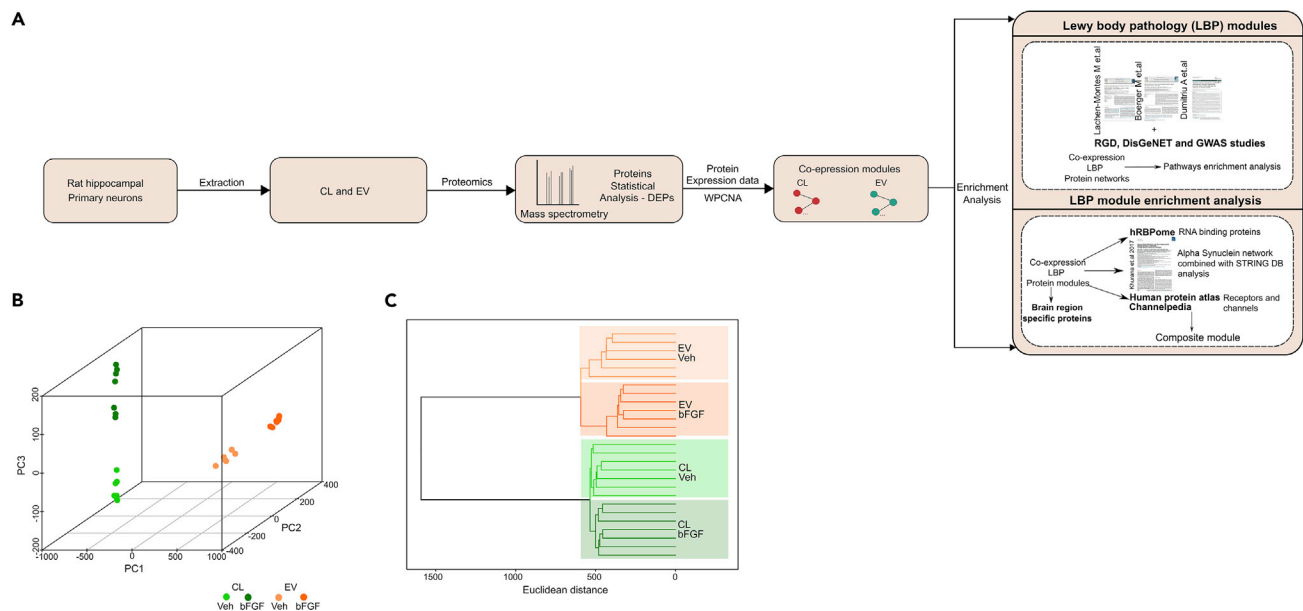https://doi.org/10.1016/j.isci.2020.101349

Figure 1. Evaluation of Proteomic Changes in bFGF-Treated Rat Brain Hippocampal Primary Neurons

(A) Schematic representation of proteomic data collection from rat hippocampal primary neurons cell lysate (CL) and extracellular vesicles (EV). The protein expression data were used to perform network and Lewy body pathology enrichment analysis.

(B) Principal component analysis (PCA) based on CL and EV pellet proteome datasets. Total three-dimensional PCA plotting as 86.8% of variance (PC1 = 82.03%, PC2 = 3.47%, PC3 = 1.37%).

(C) The dendrogram represents the hierarchical clustering based on the Euclidean distances computed from $\log_2$ LFQ intensities.

See also Figure S1.

interactions among these DEPs, we adapted a weighted protein co-expression network analysis (WPCNA) methodology and probed the subsequent co-expression modules for LBP-associated proteins. This approach allowed us to extract LBP-enriched modules and revealed the molecular interactions between bFGF signaling and LBP-associated molecular changes. We specifically identified LBP-related RNA-binding proteins (PD-RBPs), numerous ion channels and receptor proteins, and α-Syn interacting proteins as interactome components that connect bFGF signaling to α-Syn pathology. Therefore, our results will support the investigation of bFGF signaling in α-Syn-associated pathological changes.

RESULTS

Characteristic CL and EV Proteome Changes Are Induced by bFGF

In order to examine bFGF-induced proteome changes in the CL and in EVs, we treated hippocampal neurons for 24 h with bFGF (50 ng/mL) and subjected the CL and EV fraction to high-resolution mass spectrometry (MS) (see Transparent Methods for experimental details) (Figure 1A). Primary rat hippocampal neurons from E18 CD (Sprague Dawley) rat embryos were used for all experiments. All experiments were performed by using at least biological triplicates and exhibited very strong Pearson correlation coefficients (r ∼ 0.98–1) among the replicates, demonstrating a high reproducibility in both CL and EV datasets (Figures S1A and S1B). All proteins were detected at least thrice in the technical replicates of control and bFGF-treated samples. These criteria identified n = 5,314 and n = 2,258 proteins for the CL and EV fraction, respectively. We next performed an unsupervised clustering using principal component analysis (PCA) on CL and EV proteomic datasets. As expected, we found a clear separation between the two conditions (Figure 1B), and Euclidian distance-based hierarchical clustering confirmed these findings (Figure 1C). Next, we analyzed the differential expression of proteins (DEPs) to define the proteomic signature from CL and EV. This analysis yielded a set of n = 1,660 and n = 650 DEPs in CL and EV fractions (Tables S1A and S1B). Taken together, our results demonstrate that bFGF extensively affects the expression of a large number of proteins in the CL and EVs from primary hippocampal neurons.

Co-expression Analysis Organized Proteome-wide Changes in CL and EV into Modules

Next, we performed WPCNA on proteins differentially expressed in response to bFGF (Figure S2). Co-expression module analysis yielded nine CL ($M_{CL}1$–$M_{CL}9$) and four modules EV ($M_{EV}1$–$M_{EV}4$) modules
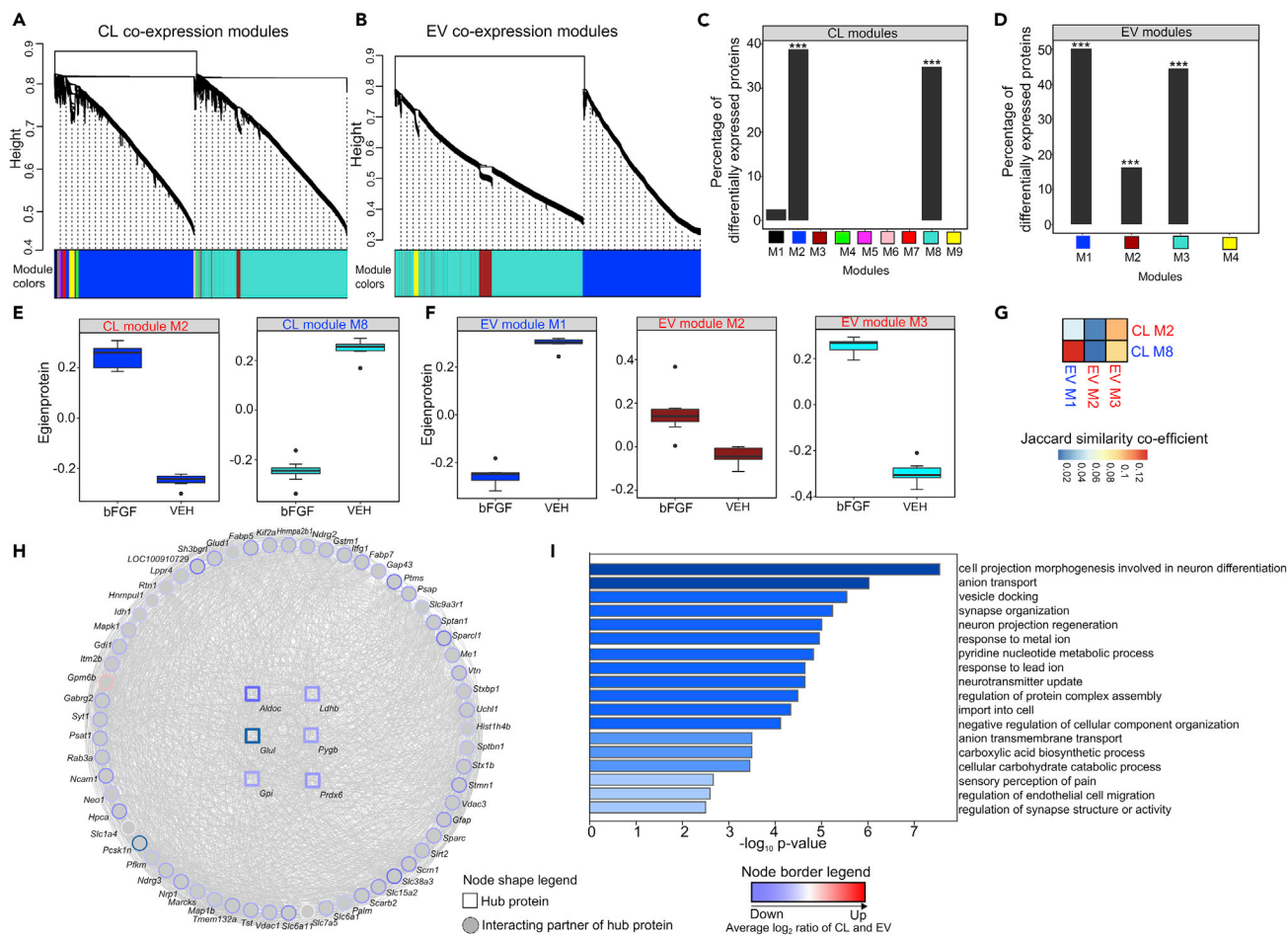
Figure 2. WPCNA Analysis of Cell Lysate (CL) and Extracellular Vesicles (EV) bFGF Induced Proteomes

(A) Dendrogram clusters CL proteins (n = 5,314) into nine modules.

(B) The dendrogram groups EV proteins (n = 2,258) into three co-expression modules.

(C and D) The bar plots represent the enrichment of differentially expressed proteins (DEP) signatures in CL and EV co-expression modules; x and y axis denote the modules and percentage overlap of the DEP signature (***$p \leq 0.01$, negative $\log_{10}$ Benjamini-Hochberg adjusted p values; Fisher's exact test).

(E and F) Module expression profiles of two CL and three EV modules (Wilcoxon test p value: 0.0034, 0.00094), respectively.

(G) Module resemblance between each set of modules was assessed by the Jaccard similarity co-efficient between their sets of CL and EV modules. See also Figures S2 and S3.

(H) The module plot shows the common module the $M_{EV}1$ and $M_{CL}8$ modules based on the high Jaccard similarity coefficient.

(I) The most significant (negative $\log_{10} p \leq 0.05$) biological processes gene ontology (GO) terms of common module between CL and EV. Note: red and blue colors indicate up- and down-regulation, respectively. Gene symbols corresponding to proteins are used as labels in the module plot.

from CL (n = 5,314) and EV (n = 2258) proteome datasets, respectively (Figures 2A and 2B). To further examine the bFGF-induced proteome signature, the statistically significant, differentially expressed proteins (sDEPs) were mapped to the co-expression modules. Among the CL modules, $M_{CL}2$ and $M_{CL}8$ depicted the highest sDEP signature (Figure 2C), and of the four EV modules, $M_{EV}1$, $M_{EV}2$, and $M_{EV}3$ were found with the strongest sDEPs signature (Figure 2D). These sDEP modules were considered for further analysis (Tables S2A and S2B). In WPCNA analysis, modules are represented by a weighted expression profile (Eigenprotein) of co-expressed proteins. To test the expression pattern of each sDEP module, we computed module Eigenprotein values and found an increased expression of proteins in $M_{CL}2$ and $M_{EV}2$ and 3 modules, whereas modules $M_{CL}8$ and $M_{EV}1$ showed a decreased expression in response to bFGF treatment (Figures 2E and 2F). An additional module preservation analysis demonstrated that co-expression modules from both datasets were strongly preserved, with a Z-summary score above 10, in comparison with random modules (Figures S3A and S3B). Next, we sought to identify the common modules and computed Jaccard similarity co-efficient between the CL and EV. This analysis indicated a higher overlap

between the M$_{EV}$1 and the M$_{CL}$8 module (Figure 2G), and both modules had down-regulated proteins in response to bFGF treatment. Next, we explored the common interactions of key regulatory proteins (so-called hubs) in the M$_{CL}$8 and M$_{EV}$1. Hub proteins play an important role in regulating biological functions and are identified in common modules by calculating the module membership (MM) of each protein combined with protein interaction network analysis (see Transparent Methods section). These analyses identified *Gpi*, *Glul*, *Aldoc*, *Ldhp*, *Pygp*, and *Prdx6* (we used the rat gene symbol nomenclature for each protein throughout the text) as the six main down-regulated hub proteins (Figure 2H). The main interaction partners of hub proteins in the corresponding CL modules were *Lrrc47*, *Cd44*, *Cald1*, *Xpo1*, *Pja2*, and *Micu2*. A pathway enrichment analysis of the common modules (M$_{CL}$8 and M$_{EV}$1) revealed a huge number of biological functions for these proteins (Figure 2I). In sum, these results provided an initial modular assessment of the bFGF-incited proteomic changes in hippocampal neurons.

Proteins Linked to Lewy Body Pathologies Are Enriched in CL and EV Co-expression Modules

We next mined the proteins that associate to Lewy body pathologies (LBPs) from the widely published PD literature and intersected them with our co-expression modules in order to explore LBP-related proteins among the bFGF-exhorted modules (Figure 1A). We endorse that associative likelihood of these results may be more for LBP due to the aforementioned clinical features of PD and primary hippocampal neurons as a source of datasets used in this study. We found M$_{CL}$2 and M$_{CL}$8 and M$_{EV}$1 and M$_{EV}$3 modules to be significantly (BH corrected p value $\leq$ 0.05) enriched with the LBP molecular signature (Figures 3A and S4). The assimilation of markers from genome-wide association studies (GWASs) and proteome-wide data permits the identification of potential molecular mechanisms in disease modules. Thus, we compiled 15 statistically significant LBP-GWAS studies (see Transparent Methods) and intersected them with bFGF-incited sDEP modules. Again, we found a higher degree of overlap with GWAS datasets in M$_{CL}$2 and 8 and in M$_{EV}$1 and 3 (Tables S3A and S3B). All LBP modules consisted of up- and down-regulated proteins further contributing to a substantial level of heterogeneity among the interacting proteins, where M$_{CL}$8 and M$_{EV}$3 were more heterogeneous as compared with M$_{CL}$2 and M$_{EV}$1 in terms of up- or down-regulated proteins (Figure S4). For a better understanding of this heterogeneity we conducted a module-wise pathway enrichment analysis revealing module-specific up- and down-regulated pathways (Figure 3B).

bFGF Modulates the Abundance of LBP-Associated RNA-Binding Proteins

Next, we examined the role of disease-associated pathological processes in these modules. Altered RNA metabolism is associated with familial PD (Lu et al., 2014). Therefore, we screened our data for LBP-related RNA-binding proteins (LBP-RBPs). This analysis revealed LBP-RBPs in the CL (M$_{CL}$2 = 8; M$_{CL}$8 = 4) and EV (M$_{EV}$1 = 3; M$_{EV}$3 = 1) modules, thus allowing us to construct LBP-RBPs interaction modules in each dataset and determine hub-RBPs along with their respective enriched pathways (Figures 3C and 3D). In the CL, *Rps6*, *Eef2*, *Srp14*, *Gspt1*, *Ddx6*, *Lars*, *Atxn2*, and *Rps14* were found as the key up-regulated LBP-RBPs, whereas *Hnrnpa2b1*, *Hnrnph3*, *Fus*, and *Ilf2* were key down-regulated LBP-RBPs. In the EV fraction, *Aco1*, *Eef2*, and *Hnrnpa2b1* were key down-regulated LBP-RBPs and *Rps14* was a key up-regulated LBP-RBP. From the cellular and subcellular location analysis of hub LBP-RBPs, we found up-regulated proteins like *Rps6* localize mainly to mitochondria, *Eef2* localizes to the plasma membrane and cytosol, *Srp14* to nucleoli, *Gspt1* and *Atxn2* to the cytosol, *Ddx6* to cytoplasmic bodies, *Lars* to nuclear bodies, and *Rps14* to the endosomal reticulum and cytosol. Most of the nucleoplasm LBP-RBPs are down-regulated except for *Eef2* (localized to the plasma membrane and cytosol) and *Aco1* (found in mitochondria and cytosol). In summary, these results suggest an effect of bFGF on a variety of LBP-associated RBPs located to distinct cellular compartments.

bFGF Predominantly Affects the Abundance of LBP-Associated Metabotropic Receptors

In addition to RBPs, neuronal ion channels and receptors contribute to α-Syn-associated pathological changes in LBP (Surmeier and Schumacker, 2013). Therefore, we next investigated the effect of bFGF on metabotropic and ionotropic receptors in our data. Two sets of (ionotropic) AMPA receptor subunits were found within the up-regulated LBP-M$_{CL}$2-module (n = 12) and in the down-regulated LBP-M$_{CL}$8 (n = 10) module with *Nptx2* (M$_{CL}$2) and *Gria1* or *Gria2* (M$_{CL}$8) as corresponding intramodular hubs. Ionotropic NMDA receptors were detected for the down-regulated LBP-M$_{CL}$8 (n = 7) module with *Grin2b* as intramodular hub. A number of up-regulated metabotropic adrenergic receptors were found in the LBP-M$_{CL}$2 (n = 20) module with *Nedd4* as an intramodular hub and down-regulated dopamine receptors were found in the LBP-M$_{CL}$8 (n = 6) module with *Cnr1* as an intramodular hub (Figure 4A). Limited LBP-related glutamate receptors were detected in the down-regulated LBP-M$_{EV}$1 (n = 2) module from the EV
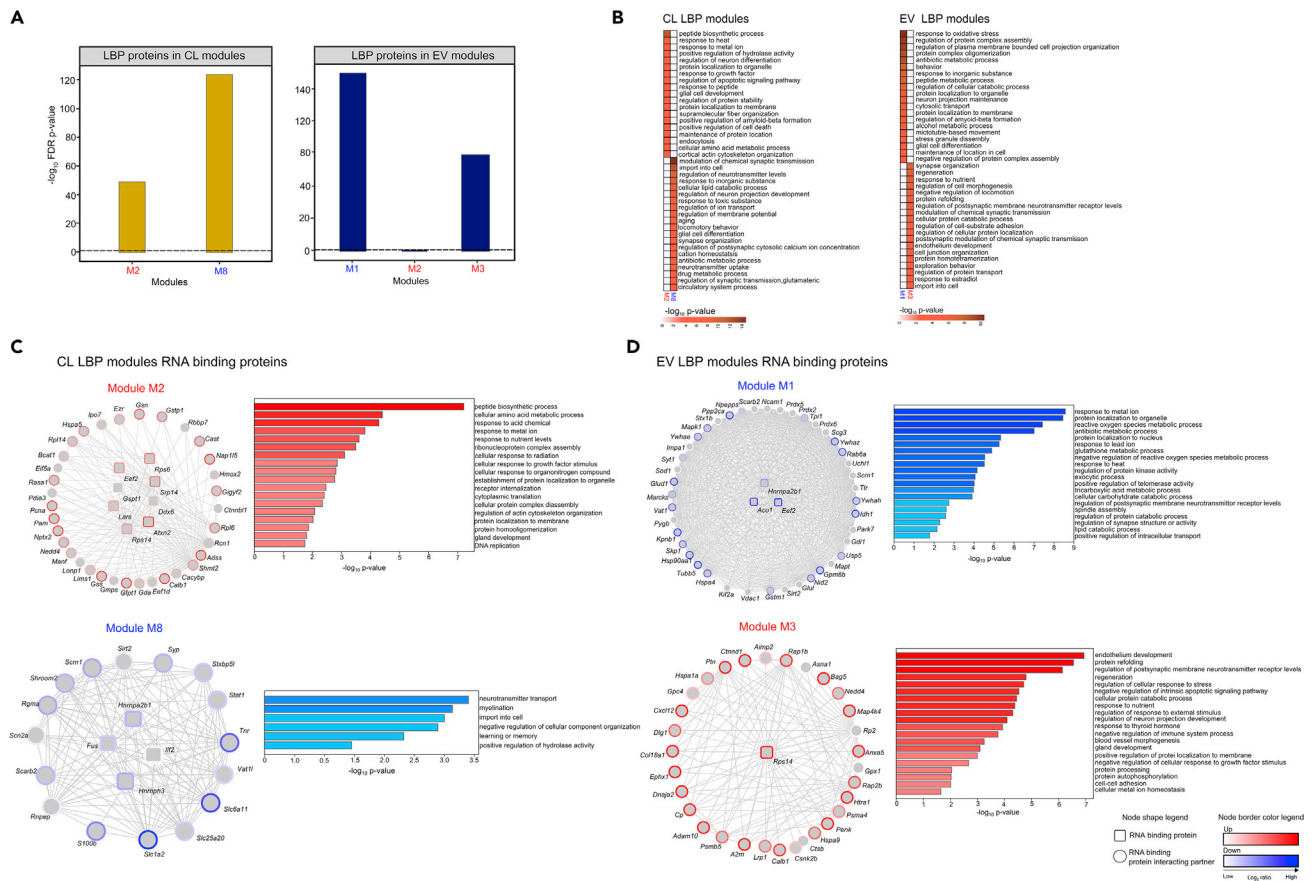
Figure 3. Enrichment of Lewy Body Pathology (LBP) Linked RNA-Binding Proteins (RBPs) in Cell Lysate (CL) and Extracellular Vesicles (EV) Co-expression Modules

(A) The bar plots show Lewy body pathology proteins enrichment in CL and EV co-expression modules. See also Figure S4 (Note: The y axis of bar plot denotes negative $\log_{10}$ Benjamini-Hochberg adjusted p values, Fisher's exact test, dotted line represents the statistical significance 1.31, is comparable with the p values ≤ 0.05).

(B) Biological processes enrichment analysis on LBP Co-expression modules both CL (left-side) and EV (right-side).

(C and D) Module plots representing the RNA-binding proteins and their interacting partners of LBP modules from both CL and EV up and down biological processes enrichment of each module. Note: Red and blue colors denote up and down-regulation, respectively. Gene symbols matching to proteins are used as labels in the LBP-RBPs modules.

fraction, whereas LBP-related adrenergic and opioid receptors were found in the up-regulated LBP-M$_{EV}$3 module (n = 7 and n = 14, respectively) (Figure 4B). The strength between the protein interactions was determined by computing a connectivity score; metabotropic adrenergic receptors and ionotropic glutamatergic AMPA receptors were strongly connected in the CL modules (Figure 4C). In the EV modules, a high connectivity was observed for metabotropic opioid and adrenergic receptors (Figure 4D). Jaccard similarity analysis enabled the identification of an up-regulated M$_{CL}$2 module and M$_{EV}$3 module as a common module, suggesting a linearized protein exodus as EV content for LBP-related receptors (Figure 4E). Only the down-regulated LBP-M$_{CL}$8 module (n = 11) has shown ion channel enrichment with slightly less down-regulation of *Scn2a* as intramodular hub (Figure 4F). Taken together, our analyses suggest that predominantly metabotropic receptor-associated molecules are pledged in response to treatment with bFGF along with a small subset of ionotropic glutamate receptors.

bFGF Influences the Molecular Assembly of α-Syn-Interaction in LBP

Among the detected ion channel receptors and channels, we found *Nedd4* and *Tln1* as key α-Syn interaction partners. Because of the α-Syn role in LBP the dataset was examined for additional α-Syn interaction partners (Figure 5A). We identified α-Syn interacting proteins in our LBP modules using information reported in Khurana et al. (2017); this protruded to a α-Syn interaction network (pSIN) (Figure 5B). There were 20 overlapping proteins
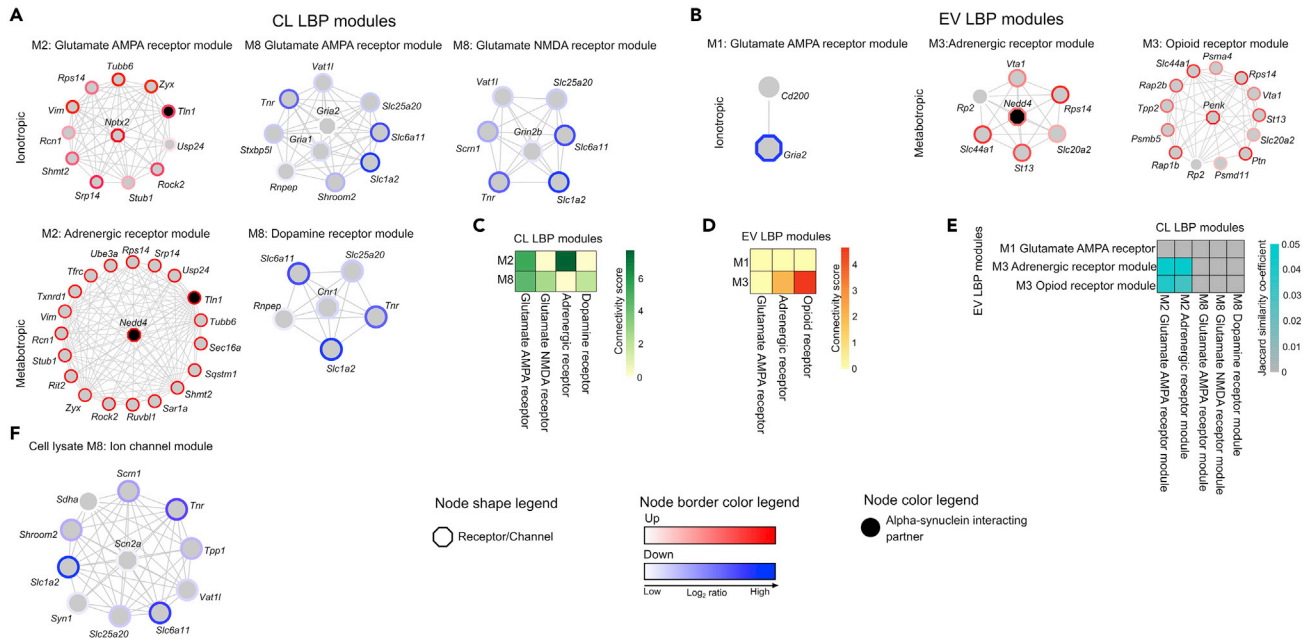
Figure 4. Association of Ionotropic, Metabotropic Receptors and Ion Channel in Lewy Body Pathology (LBP) Modules
(A and B) The module plots show CL and EV LBP ionotropic and metabotropic receptor and their interacting partners. Note: Edges/interactions between the proteins (gene symbols corresponding to proteins are used as labels) represent the correlation between them.
(C and D) Connection strength of ionotropic, metabotropic receptors (CL, EV) modules analyzed using connectivity score represented as a pairwise matrix.
(E) Pairwise similarity of ionotropic, metabotropic receptors between the CL and EV LBP modules was evaluated using Jaccard similarity co-efficient.
(F) The module view of the CL LBP ion channel and its interactions.

in all modules of which 3 overlapped between EV and pSIN, 8 between CL-pSIN, 106 between EV-CL PD-modules, and 9 (*Vdac1, Abca1, Rab6a, Nucb1, Aldh2, Nedd4, Tln1, Mapk1,* and *Rps14*) among all subsets (Figure 5B) (Table S4). For a comprehensive sketch of these protein interactions, we further examined 50 immediate interactions of the overlapping 115 proteins, obtaining an α-Syn interaction network using STRING database (Figures S5A and S5B). In order to further examine the interactome between LBP and bFGF signaling, we developed an overall composite module (CM) among LBP-associated receptors, ion channels, RBPs, α-Syn interacting partners, and key players in the EV-CL modules (Figure 5C). The CM was heterogeneously composed of both up-/down-regulated proteins and key proteins that were extracted from CM by estimating various centrality dimensions (Figure S6). This comprehensive centrality analysis has concluded the shortest-path-betweenness-centrality as a key parameter. This enabled us to mine the top 5% informative proteins, including *Scrn1, Slc6a11, Slc1a2, Tnr* (down-regulated) and *Rps14, Vim, Slc44a1* (up-regulated) (Figure 5D). The functional enrichment of the composite module was further characterized by pathway enrichment analysis (Figure 5E). Based on these results, we concluded that these proteins represent key components of the molecular interface of bFGF-signaling and LBP.

bFGF-Enhanced EV-Release Possibly Supplements LBP Progression

Because of the sequential progression of pathology to defined brain regions in LBP, we finally mapped the presence of LBP module proteins to major brain regions suggested in Sharma et al. (2015) (Figures 6A and S7). LBP modules from CL and EV were appreciated in brain regions like the optic nerve, cerebellum, corpus callosum, olfactory lobe, brain stem and hippocampus. Conversely, we did not find a significant amount of proteins matched for the prefrontal cortex, striatum, and thalamus. We attributed this to sample collection from hippocampal neurons and, possibly, to variations in rat and mouse proteomic homologs. Within LBP proteins of various brain regions, we examined the coherent candidates in CL-EV modules (Figure 6B). For the cerebellum, we found a total number of 30 proteins in both CL-EV LBP-modules, and among these, two were shared with an overall partaking candidature of 6.67% for the designated brain region. Similarly, in the corpus callosum (25 proteins; 4 shared in the EV-CL PD-modules), optic nerve (72 proteins; 4 shared), hippocampus (23 proteins; 2 shared), and olfactory bulb (13 proteins; 2 shared) have earned an overall candidature of 16%, 5.56%, 8.7%, and 15.38% respectively. We made use of these shared candidates (Table S5) to
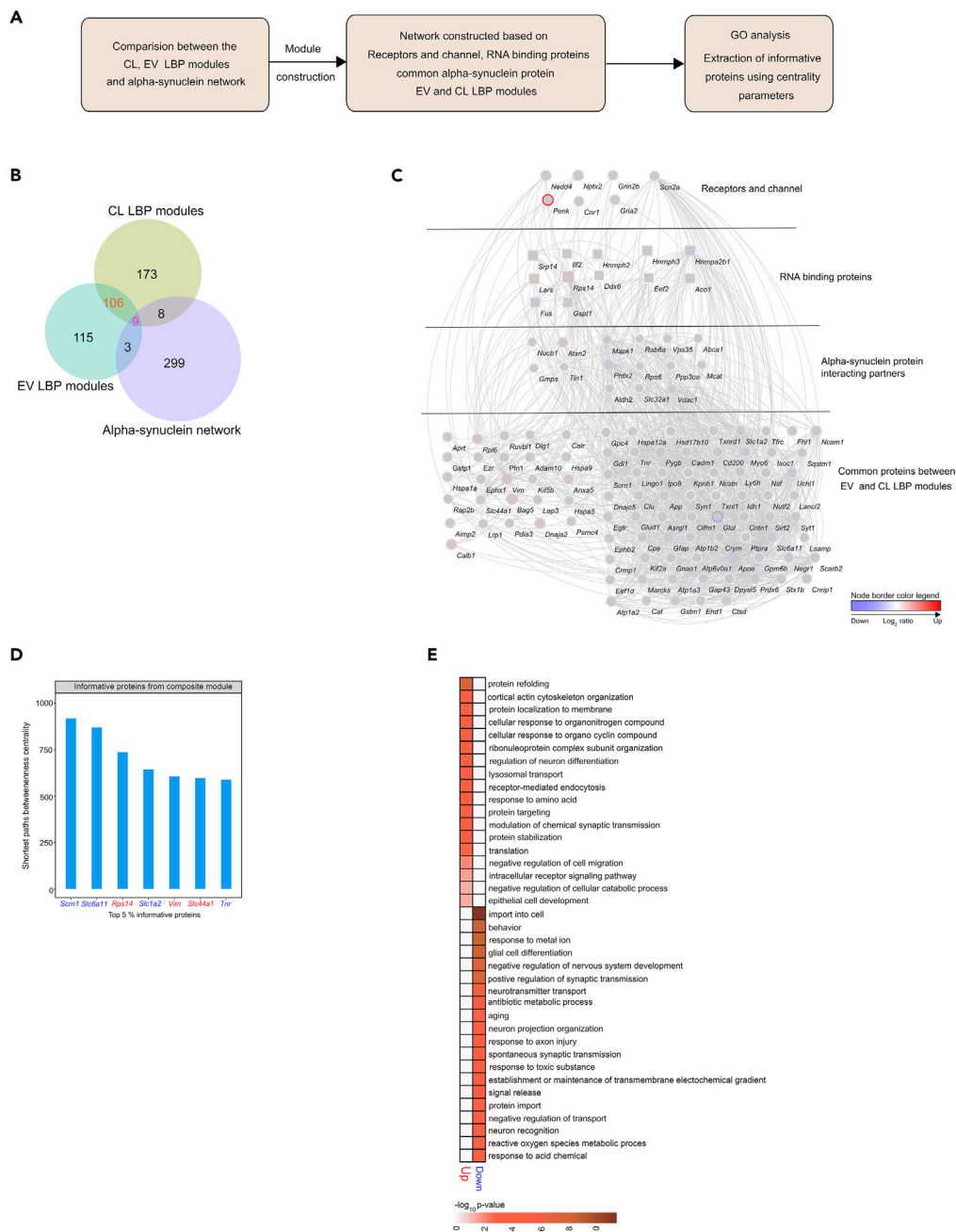
Figure 5. Amelioration of Alpha-Synuclein (α-Syn) Protein and Construction of Composite LBP Module

(A) Outline describing the workflow for generating common modules.

(B) Venn diagram showing the overlap between the LBP module proteins from CL, EV, and alpha-synuclein protein interacting partners.

(C) A composite LBP co-expression module (CM) illustrating the interactions between the common LBP proteins from common CL, EV, alpha-synuclein protein interacting partners and receptors, ion channel, RNA-binding proteins. See also Figure S6.

(D) The bar plot shows the top 5% of informative proteins from the composite module based on the shortest path betweenness centrality.

(E) The statistically significant (negative log$_{10}$ p value ≤ 0.05, hypergeometric test from METASCAPE) biological processes enrichment of the composite LBP module. Note: Red and blue color denote up- and down-regulation, respectively. Gene symbols related to proteins are used as labels in the CM plot.
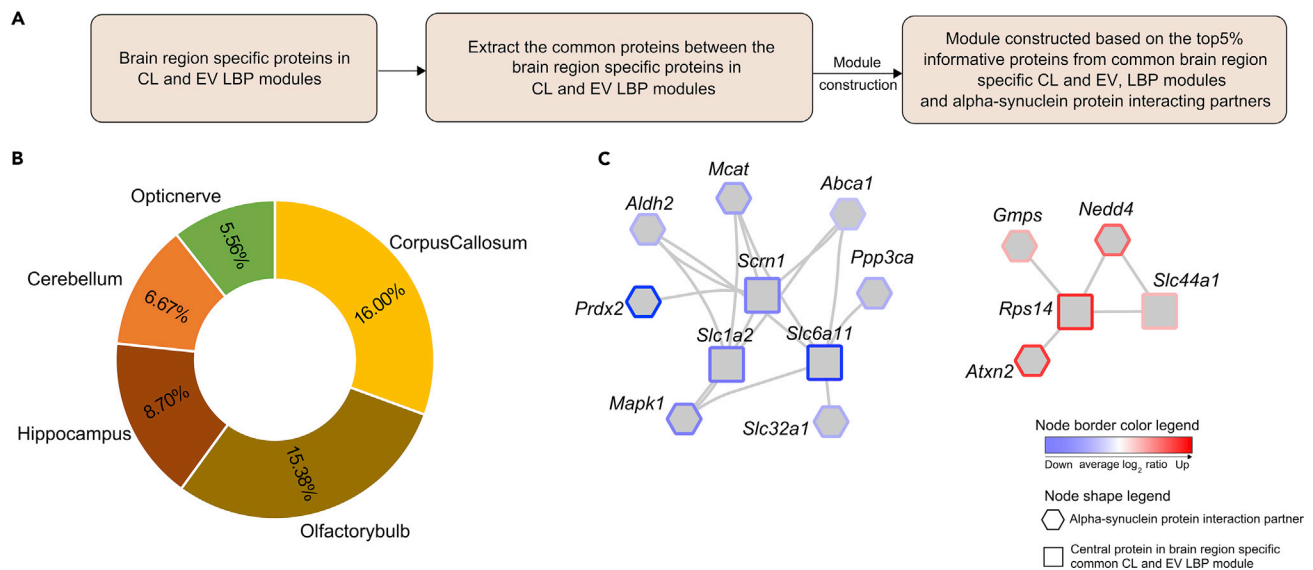
Figure 6. Influence of α-Syn Protein Interactions in Brain-Specific Regions

(A) Schematic representation of the workflow to generate brain region-specific LBP modules.

(B) Doughnut plot shows the percentages of common brain region-specific proteins between the CL and EV LBP modules. See also Figure S7.

(C) The module characterizes interactions between top 5% informative proteins of common brain region-specific module and their interactions with alpha-synuclein protein interacting partners. Note: Gene symbols associated to proteins are used as labels in the modules.

See also Figure S8.

develop a composite protein interaction module (CPIM) along with the α-Syn interacting partners and other common PD proteins of EV-CL (Figures S8A and S8B). By assessing the centrality parameters (Figure S8C) we identified the top 5% informative proteins of CPIM based on shortest path betweenness centrality. *Scrn1*, *Slc6a11*, *Slc1a2*, and *Tnr* were among the top down-regulated and *Slc44a1*, *Rps14* were the most informative up-regulated proteins in the CPIM (Figure S8D). Submodular analysis revealed *Aldh2*, *Mcat*, *Abca1*, *Ppp3ca*, *Slc32a1*, *Mapk1,* and *Prdx2* as top α-Syn interacting proteins, supporting a bilateral interaction with the most informative top down-regulated proteins identified in CPIM and *Atxn2, Gmps, Nedd4* as α-Syn-related interactions with top most informative up-regulated proteins (Figures 6C and S8E). We counter-validated the implications of bFGF-induced expression in our study and found up-regulated modules M$_{CL}$2 and M$_{EV}$3 significantly enriched for pathology associated hub-molecules identified in postmortem brain tissues of patients with LB disease (Figures S9A and S9B). Taken together, these results imply that, in a disease state an EV-mediated cross talk among various brain regions is supported from these results, which could involve transport of misfolded proteins via EVs and can affect the protein metabolism beyond the host at recipient brain region eventually claiming shutdown of neuronal molecular mechanisms and neurodegeneration.

DISCUSSION

Here we performed a global proteomic evaluation of bFGF effect induced to the CL and EV fractions from cultured hippocampal neurons and reasoned out its relevance in LBP (Figure 1). Instead of individual protein analysis, we rather applied a system-level comprehensive approach to examine bFGF-regulated DEPs using WPCNA (Figure 2). Because of the role of neurotrophic factors in hippocampal pathology, we screened our WPCNA-derived modules for proteins linked to LBP-associated molecular changes. This strategy enabled us to capture LBP modules (Figures 3A and Tables S3A and S3B) and allowed intersecting bFGF- with LBP-related proteome changes. Our data identified n = 532, bFGF-induced DEPs associated to LBP molecular changes thus revealing a molecular network of LBP-associated proteins and their modulation by bFGF in hippocampal neurons. Our results will therefore support the investigation of neurotrophic signaling in LBP pathology onset and progression.

The top 5% up-regulated α-Syn interacting proteins shown in our results were *Rps14, Vim*, and *Slc44a1* (Figure 5D). Ribosomal protein *Rps14* has been reported to be differentially regulated in mitochondria of

neural stem cells from patients with PD; under ribosomal stress this protein contributes to mitochondrial fragmentation (Zhou et al., 2015). Similar to PD-GWASs (Iwaki et al., 2019) our analysis confirms the up-regulation of the *Slc44a1* (choline transporter-like protein-1) in response to bFGF treatment. It is shown that *Slc44a1* might be involved in mitochondrial energy metabolism (Michel and Bakovic, 2009). Remarkably, a decrease of choline uptake reported in old adults (Cohen et al., 1995) and in α-Syn overexpressing animals (Wassouf et al., 2019) further establishes the association of bFGF-induced proteomic changes to LBP. Finally, up-regulation of *Vim* in response to bFGF is correlated with PD (van den Berge et al., 2012). *Scrn1, Slc6a11, Slc1a2,* and *Tnr* were among the top down-regulated CPIM proteins. In line with its role in PD, *Scrn1* is another α-Syn interaction partner involved in synaptic vesicle recycling, ER modulation, and calcium homeostasis (Lindhout et al., 2019). *Scrn1* interactions with the vesicle-associated membrane protein (VAMP)-associated protein (VAP) and association of VAP low levels in PD further suggest a pathological relevance for *Scrn1* (Murphy and Levine, 2016). In summary, these proteins are strongly associated with PD and their modulation by bFGF may provide more molecular substrates for the effect of bFGF in LBP. *Slc1a2* has been investigated for polymorphic associations with PD (Appenzeller et al., 2013). *Slc6a11* has been demonstrated to modulate basal ganglia neuronal networks (Chazalon et al., 2018), and *Tnr* may likewise contribute to PD pathology (Tsai et al., 2014). In conclusion, these results will provide the molecular basis for further studies to address the role of bFGF-induced proteomic changes in LBP.

In addition to the CPIM-derived top 5%, numerous additional candidate genes from our data have a potential pathogenic relevance for LBP. For instance, our data demonstrated an up-regulation of *Nptx2* (Figure 4A). This protein is involved in excitatory synapse formation. It also plays a role in clustering of AMPA-type glutamate receptors at established synapses, resulting in non-apoptotic cell death of dopaminergic nerve cells. In accord with the relevance of glutamate receptors, we found a down-regulation of AMPA (*Gria1* and *Gria2*) and NMDA (*Grin2b*) receptors, which is associated with the accelerated aging of neurons (Dryanovski et al., 2013). Likewise, we found a down-regulation of the glutamate transporter 2 gene *Slc1a2*, possibly further contributing to a dysregulated glutamate metabolism. Notably, *Nptx2* has been found to be present in LBs of patients with PD (Moran et al., 2008), possibly implicating bFGF signaling in LB formation. Another example comes from the alterations of the mTOR and growth factor signaling pathways (Lynch-Day et al., 2012) and impaired autophagy in LBP. Earlier, we confirmed the role of *Nedd4*-family E3 ligases in mTOR signaling (Hsia et al., 2014) and it has been reported that the ubiquitination of *Nedd4* by E3-ligases controls autophagy mechanisms (Sun et al., 2017) and activation of the inflammasome (Liu et al., 2019). Up-regulation of *Nedd4* in our data (Figures 4A and 4B) thus implicates the role of bFGF in modulating autophagy during LBP. In accord, *Nedd4* ubiquitination has been shown to suppress autophagy in neuroblastoma cells (Xu et al., 2017) possibly impairing neuronal clearance mechanisms. Furthermore, *Nedd4* ligases rapidly promote ubiquitination of α-Syn (Mund et al., 2018), further supporting a role of bFGF in α-Syn-mediated pathogenic mechanisms. In concurrence to such hypothesis, we observed new and formerly unknown interactions of *Tln1* (up-regulated) with *Nedd4* and *Nptx2* (Figure 4A). *Tln1* is known as integrin-associated cytoskeletal protein and has binding sites for other cytoskeletal proteins such as α-*Synemin*, helping them to unfold. In addition, *Tln1* regulates functions like cell proliferation, survival, and migration (Roberts and Critchley, 2009). The upstream and downstream status of these proteins requires a further validation and may support the understanding of protein misfolding mechanisms (Moran et al., 2008).

Interestingly, many of these LBP-associated proteins exhibited a similar behavior in the CL and EV fraction, i.e., up-regulated CL proteins were up-regulated in the EV fraction and vice versa. We attribute this finding to the mechanism of EV formation during the generation of multivesicular bodies (MVBs), where highly abundant proteins are more likely to be excreted by EVs (Gruenberg et al., 1989). In accord with an EV-mediated transmission of LBP-associated proteins, our data suggest a high representation of the top 5% proteins in CPIM and CM for olfactory bulb (OB) and corpus callosum (CC) (Figures 6B and 6C) (Zapiec et al., 2017; Niu et al., 2018), suggesting a connection of the pathogenic molecular network between these regions. In accord, the OB is considered as an entry for environmental pathogens that may induce LBP changes in the OB that are then transmitted to central brain areas, as an occurrence via EVs (Braak and Del Tredici, 2009). Along these lines, the loss of CC volume in patients with PD has been associated with cognitive impairment (Goldman et al., 2017).

Taken together, our study identifies a number of proteomic network changes and individual protein candidates that result from growth factor signaling and their potential contribution to LBP. Future

experimental studies should investigate these candidates and assess their contribution to Lewy body-associated pathological changes *in vitro* and *in vivo*. This will ultimately strengthen the connection between growth factor signaling and LBP and allow assessment of growth factor signaling as a potential therapeutic target in LBP. In summary, these results will support the examination of bFGF for modulating disease progression in LBP and its cell-to-cell spreading, which has become a common theme for understanding disease progression in neurodegenerative conditions.

Limitations of the Study

A limitation of our study is the absence of wet-lab experimental data from an LBP disease model. However, there is currently no rat model that replicates Lewy pathology well in its complexity (Rockenstein et al., 2002; Hashimoto et al., 2003). Because our earlier results on the effect of bFGF (Kumar et al., 2020b) were derived from rat neurons, using more abundant mouse models would add additional bias. Taken together, we thus believe that intersecting "real-world" human proteomic alterations derived from databases with the effects of growth factor treatment in healthy rat primary neurons allows for a less confounded investigation of its true cellular effects. Future studies should validate our results in experimental disease model *in vitro* and *in vivo* as well as in postmortem material from human cases.

Resource Availability

Lead Contact

Any questions or requests should be addressed to the Lead Contact (thomas.koeglsperger@dzne.de).

Materials Availability

We used the proteome data as mentioned below. This study did not generate new reagents.

Data and Code Availability

We deposited the proteome datasets in the ProteomeXchange Consortium via the PRIDE partner repository, CL dataset identifier PXD015969 and EV dataset identifier PXD014401. We used published algorithms without generating new computer code.

METHODS

All methods can be found in the accompanying Transparent Methods supplemental file.

SUPPLEMENTAL INFORMATION

Supplemental Information can be found online at https://doi.org/10.1016/j.isci.2020.101349.

AUTHOR CONTRIBUTIONS

Conceptualization, R.K.; Methodology, R.K and S.D.; Software, R.K. and S.D.; Formal Analysis, R.K., S.D. and T.K.; Investigation, R.K., S.D., and S.A.M.; Data Curation, R.K., S.D., and S.A.M.; Writing – Review and Editing, R.K., S.D., S.M. and T.K.; Supervision and Funding Acquisition, T.K., S.F.L., K.B. and G.U.H.

DECLARATIONS OF INTERESTS

The authors declare no competing interests.

CellPress
OPEN ACCESS

REFERENCES

Appenzeller, S., Schulte, C., Thier, S., Hopfner, F., Pendziwiat, M., Papengut, F., Klein, C., Hagenah, J., Kasten, M., Srulijes, K., et al. (2013). No association between polymorphisms in the glutamate transporter SLC1A2 and Parkinson's disease. Mov. Disord. 28, 1305–1306.

Braak, H., and Del Tredici, K. (2009). Neuroanatomy and pathology of sporadic Parkinson's disease. Adv. Anat. Embryol. Cell Biol. 201, 1–119.

Chazalon, M., Paredes-Rodriguez, E., Morin, S., Martinez, A., Cristóvão-Ferreira, S., Vaz, S., Sebastiao, A., Panatier, A., Boué-Grabot, E., Miguelez, C., and Baufreton, J. (2018). GAT-3 dysfunction generates tonic inhibition in external globus pallidus neurons in parkinsonian rodents. Cell Rep. 23, 1678–1690.

Cohen, B.M., Renshaw, P.F., Stoll, A.L., Wurtman, R.J., Yurgelun-Todd, D., and Babb, S.M. (1995). Decreased brain choline uptake in older adults: an in vivo proton magnetic resonance spectroscopy study. JAMA 274, 902–907.

Deng, Z., Deng, S., Zhang, M.-R., and Tang, M.-M. (2019). Fibroblast growth factors in depression. Front. Pharmacol. 10, 60.

Dryanovski, D.I., Guzman, J.N., Xie, Z., Galteri, D.J., Volpicelli-Daley, L.A., Lee, V.M., Miller, R.J., Schumacker, P.T., and Surmeier, D.J. (2013). Calcium entry and alpha-synuclein inclusions elevate dendritic mitochondrial oxidant stress in dopaminergic neurons. J. Neurosci. 33, 10154–10164.

Fagel, D.M., Ganat, Y., Cheng, E., Silbereis, J., Ohkubo, Y., Ment, L.R., and Vaccarino, F.M. (2009). Fgfr1 is required for cortical regeneration and repair after perinatal hypoxia. J. Neurosci. 29, 1202.

Galasko, D. (2017). Lewy body disorders. Neurol. Clin. 35, 325–338.

Goldman, J.G., Bledsoe, I.O., Merkitch, D., Dinh, V., Bernard, B., and Stebbins, G.T. (2017). Corpus callosal atrophy and associations with cognitive impairment in Parkinson disease. Neurology 88, 1265–1272.

Gruenberg, J., Griffiths, G., and Howell, K.E. (1989). Characterization of the early endosome and putative endocytic carrier vesicles in vivo and with an assay of vesicle fusion in vitro. J. Cell Biol. 108, 1301–1316.

Guillemot, F., and Zimmer, C. (2011). From cradle to grave: the multiple roles of fibroblast growth factors in neural development. Neuron 71, 574–588.

Hashimoto, M., Rockenstein, E., and Masliah, E. (2003). Transgenic models of alpha-synuclein pathology: past, present, and future. Ann. N. Y Acad. Sci. 991, 171–188.

Hsia, H.-E., Kumar, R., Luca, R., Takeda, M., Courchet, J., Nakashima, J., Wu, S., Goebbels, S., An, W., Eickholt, B.J., et al. (2014). Ubiquitin E3 ligase Nedd4-1 acts as a downstream target of PI3K/PTEN-mTORC1 signaling to promote neurite growth. Proc. Natl. Acad. Sci. U S A 111, 13205.

Iwaki, H., Blauwendraat, C., Leonard, H.L., Kim, J.J., Liu, G., Maple-Grødem, J., Corvol, J.-C., Pihlstrøm, L., Van Nimwegen, M., Hutten, S.J., et al. (2019). Genomewide association study of Parkinson's disease clinical biomarkers in 12 longitudinal patients' cohorts. Mov. Disord. 34, 1839–1850.

Khurana, V., Peng, J., Chung, C.Y., Auluck, P.K., Fanning, S., Tardiff, D.F., Bartels, T., Koeva, M., Eichhorn, S.W., Benyamini, H., et al. (2017). Genome-scale networks link neurodegenerative disease genes to alpha-synuclein through specific molecular pathways. Cell Syst. 4, 157–170.e14.

Kumar, R., Tang, Q., Müller, S.A., Gao, P., Mahlstedt, D., Zampagni, S., Tan, Y., Klingl, A., Bötzel, K., Lichtenthaler, S.F., et al. (2020a). FGF2-mediated regulation of exosome release depends on VAMPs/cellubrevin in cultured hippocampal neurons. Adv. Sci. 7, 1902372.

Kumar, R., Tang, Q., Müller, S.A., Gao, P., Mahlstedt, D., Zampagni, S., Tan, Y., Klingl, A., Bötzel, K., Lichtenthaler, S.F., et al. (2020b). Fibroblast growth factor 2-mediated regulation of neuronal exosome release depends on VAMP3/cellubrevin in hippocampal neurons. Adv. Sci. 7, 1902372.

Lindhout, F.W., Cao, Y., Kevenaar, J.T., Bodzęta, A., Stucchi, R., Boumpoutsari, M.M., Katrukha, E.A., Altelaar, M., Macgillavry, H.D., and Hoogenraad, C.C. (2019). VAP-SCRN1 interaction regulates dynamic endoplasmic reticulum remodeling and presynaptic function. EMBO J. 0, e101345.

Liu, Q., Zhang, S., Sun, Z., Guo, X., and Zhou, H. (2019). E3 ubiquitin ligase Nedd4 is a key negative regulator for non-canonical inflammasome activation. Cell Death Differ. 26, 2386–2399.

Lu, B., Gehrke, S., and Wu, Z. (2014). RNA metabolism in the pathogenesis of Parkinson's disease. Brain Res. 1584, 105–115.

Lynch-Day, M.A., Mao, K., Wang, K., Zhao, M., and Klionsky, D.J. (2012). The role of autophagy in Parkinson's disease. Cold Spring Harb. Perspect. Med. 2, a009357.

McKeith, I.G., Boeve, B.F., Dickson, D.W., Halliday, G., Taylor, J.-P., Weintraub, D., Aarsland, D., Galvin, J., Attems, J., Ballard, C.G., et al. (2017). Diagnosis and management of dementia with Lewy bodies. Neurology 89, 88.

Michel, V., and Bakovic, M. (2009). The solute carrier 44A1 is a mitochondrial protein and mediates choline transport. FASEB J. 23, 2749–2758.

Moran, L.B., Hickey, L., Michael, G.J., Derkacs, M., Christian, L.M., Kalaitzakis, M.E., Pearce, R.K.B., and Graeber, M.B. (2008). Neuronal pentraxin II is highly upregulated in Parkinson's disease and a novel component of Lewy bodies. Acta Neuropathol. 115, 471–478.

Mund, T., Masuda-Suzukake, M., Goedert, M., and Pelham, H.R. (2018). Ubiquitination of alpha-synuclein filaments by Nedd4 ligases. PLoS One 13, e0200763.

Murphy, S.E., and Levine, T.P. (2016). VAP, a versatile access point for the endoplasmic reticulum: review and analysis of FFAT-like motifs in the VAPome. Biochim. Biophys. Acta 1861, 952–961.

Niu, H., Shen, L., Li, T., Ren, C., Ding, S., Wang, L., Zhang, Z., Liu, X., Zhang, Q., Geng, D., et al. (2018). Alpha-synuclein overexpression in the olfactory bulb initiates prodromal symptoms and pathology of Parkinson's disease. Transl. Neurodegener. 7, 25.

Roberts, G.C.K., and Critchley, D.R. (2009). Structural and biophysical properties of the integrin-associated cytoskeletal protein talin. Biophys. Rev. 1, 61–69.

Rockenstein, E., Mallory, M., Hashimoto, M., Song, D., Shults, C.W., Lang, I., and Masliah, E. (2002). Differential neuropathological alterations in transgenic mice expressing alpha-synuclein from the platelet-derived growth factor and Thy-1 promoters. J. Neurosci. Res. 68, 568–578.

Shahmoradian, S.H., Lewis, A.J., Genoud, C., Hench, J., Moors, T.E., Navarro, P.P., Castaño-Díez, D., Schweighauser, G., Graff-Meyer, A., Goldie, K.N., et al. (2019). Lewy pathology in Parkinson's disease consists of crowded organelles and lipid membranes. Nat. Neurosci. 22, 1099–1109.

Sharma, K., Schmitt, S., Bergner, C.G., Tyanova, S., Kannaiyan, N., Manrique-Hoyos, N., Kongi, K., Cantuti, L., Hanisch, U.K., Philips, M.A., et al. (2015). Cell type- and brain region-resolved mouse brain proteome. Nat. Neurosci. 18, 1819–1831.

Spillantini, M.G., Schmidt, M.L., Lee, V.M.Y., Trojanowski, J.Q., Jakes, R., and Goedert, M. (1997). α-Synuclein in Lewy bodies. Nature 388, 839–840.

Sun, A., Wei, J., Childress, C., Shaw, J.H., Peng, K., Shao, G., Yang, W., and Lin, Q. (2017). The E3 ubiquitin ligase NEDD4 is an LC3-interactive protein and regulates autophagy. Autophagy 13, 522–537.

Surmeier, D.J., and Schumacker, P.T. (2013). Calcium, bioenergetics, and neuronal vulnerability in Parkinson's disease. J. Biol. Chem. 288, 10736–10741.

Timmer, M., Müller-Ostermeyer, F., Kloth, V., Winkler, C., Grothe, C., and Nikkhah, G. (2004). Enhanced survival, reinnervation, and functional recovery of intrastriatal dopamine grafts co-transplanted with Schwann cells overexpressing high molecular weight FGF-2 isoforms. Exp. Neurol. *187*, 118–136.

Tsai, H.-L., Chiu, W.-T., Fang, C.-L., Hwang, S.-M., Renshaw, P.F., and Lai, W.-F.T. (2014). Different forms of tenascin-C with tenascin-R regulate neural differentiation in bone marrow-derived human mesenchymal stem cells. Tissue Eng. A *20*, 1908–1921.

Turner, C.A., Watson, S.J., and Akil, H. (2012). The fibroblast growth factor family: neuromodulation of affective behavior. Neuron *76*, 160–174.

van den Berge, S.A., Kevenaar, J.T., Sluijs, J.A., and Hol, E.M. (2012). Dementia in Parkinson's disease correlates with α-synuclein pathology but not with cortical astrogliosis. Parkinson's Dis. *2012*, 420957.

Wassouf, Z., Hentrich, T., Casadei, N., Jaumann, M., Knipper, M., Riess, O., and Schulze-Hentrich, J.M. (2019). Distinct stress response and altered striatal transcriptome in alpha-synuclein overexpressing mice. Front. Neurosci. *12*, 1033.

Xu, Q., Zhu, N., Chen, S., Zhao, P., Ren, H., Zhu, S., Tang, H., Zhu, Y., and Qi, Z. (2017). E3 ubiquitin ligase Nedd4 promotes Japanese encephalitis virus replication by suppressing autophagy in human neuroblastoma cells. Sci. Rep. *7*, 45375.

Yoshimura, S., Takagi, Y., Harada, J., Teramoto, T., Thomas, S.S., Waeber, C., Bakowska, J.C., Breakefield, X.O., and Moskowitz, M.A. (2001). FGF-2 regulation of neurogenesis in adult hippocampus after brain injury. Proc. Natl. Acad. Sci. U S A *98*, 5874.

Zapiec, B., Dieriks, B.V., Tan, S., Faull, R.L.M., Mombaerts, P., and Curtis, M.A. (2017). A ventral glomerular deficit in Parkinson's disease revealed by whole olfactory bulb reconstruction. Brain *140*, 2722–2736.

Zhou, X., Liao, W.-J., Liao, J.-M., Liao, P., and Lu, H. (2015). Ribosomal proteins: functions beyond the ribosome. J. Mol. Cell Biol. *7*, 92–104.

Supplemental Information

Basic Fibroblast Growth Factor 2-Induced

Proteome Changes Endorse Lewy Body

Pathology in Hippocampal Neurons

Rohit Kumar, Sainitin Donakonda, Stephan A. Müller, Stefan F. Lichtenthaler, Kai Bötzel, Günter U. Höglinger, and Thomas Koeglsperger
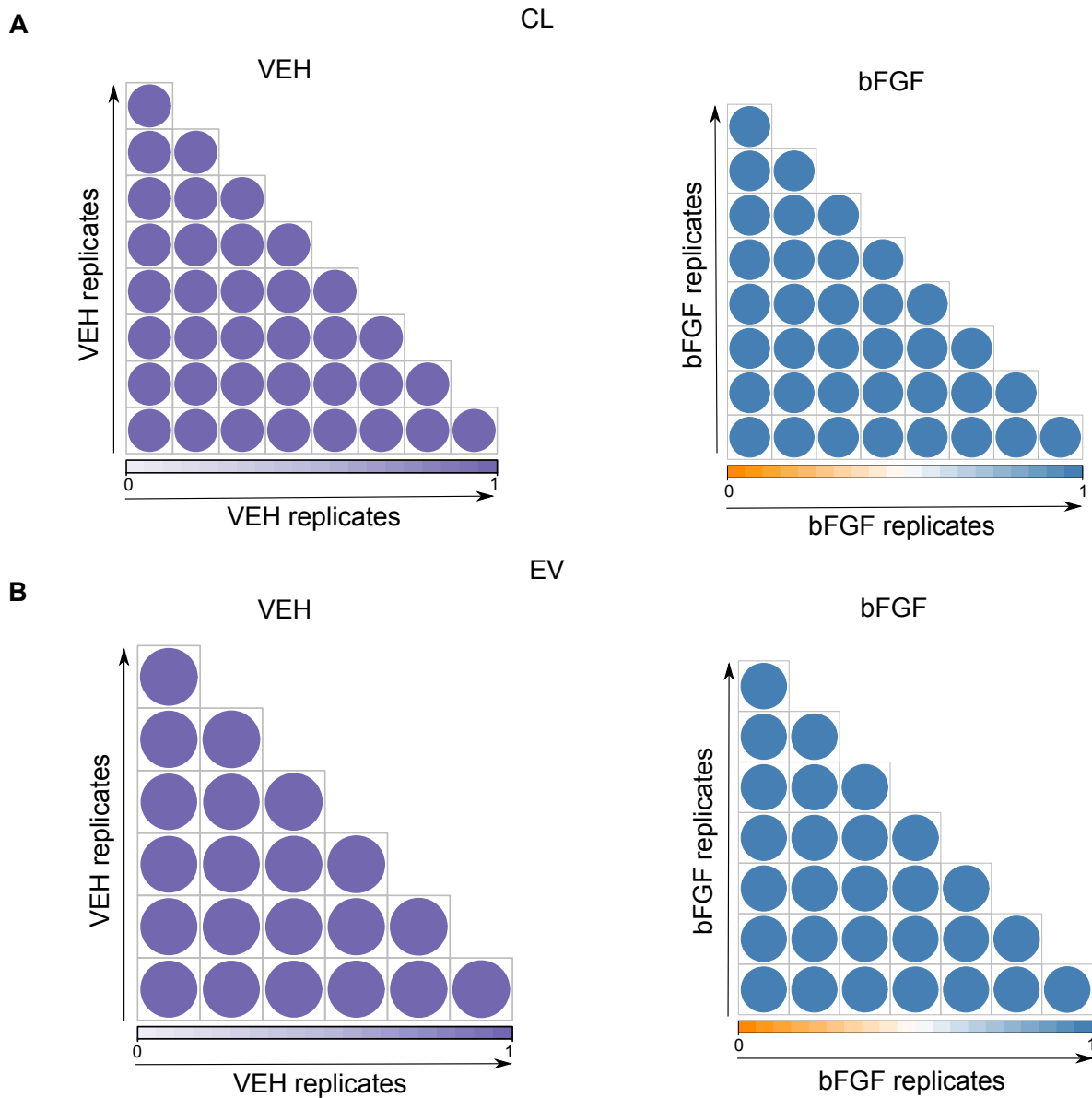
Figure S1. Correlation of proteome data sets, Related to Figure 1. (**A and B**) The heatmaps represent the correlation analysis between biological replicates of cell lysate (CL) and extracellular vesicles (EV) from control (VEH) and bFGF-treated neurons.
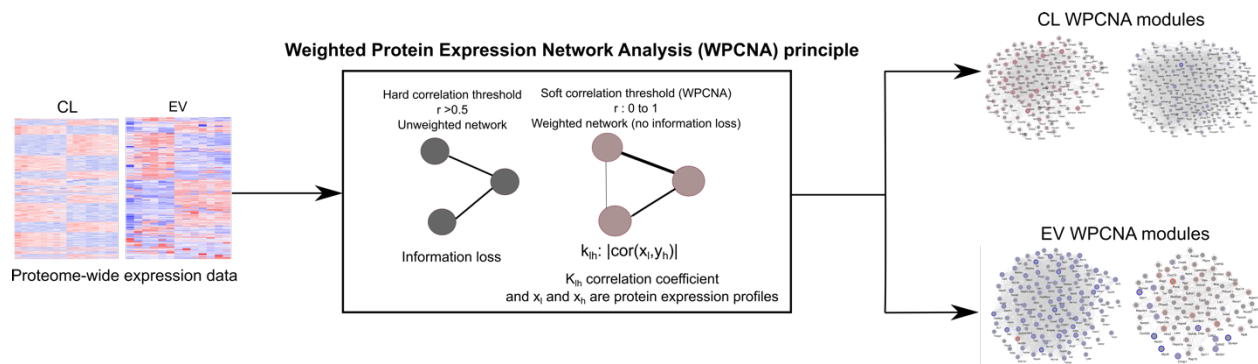
Figure S2. Schematic representation of the weighted protein expression network analysis workflow of cell lysate (CL) and extracellular vesicles (EV) protein expression modules, Related to Figure 2.

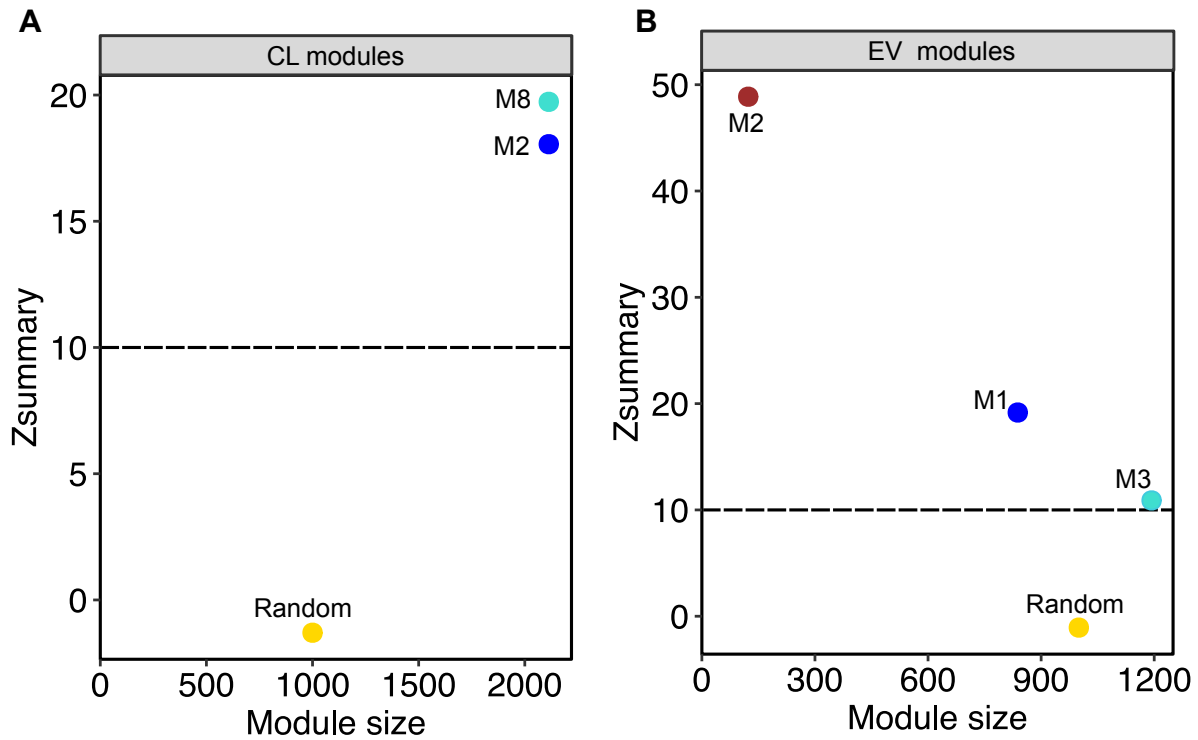**Figure S3. Cell lysate (CL) and extracellular vesicles (EV) modules preservation analysis, Related to Figure 2.** (**A and B**) Scatter plots show module preservation assessment of CL and EV LBP modules in comparison to random modules. Less than 0 represents no preservation; 0–2, weak preservation; 2–10, moderate preservation; and more than 10, high preservation. Black dotted line represents the high preservation of modules.
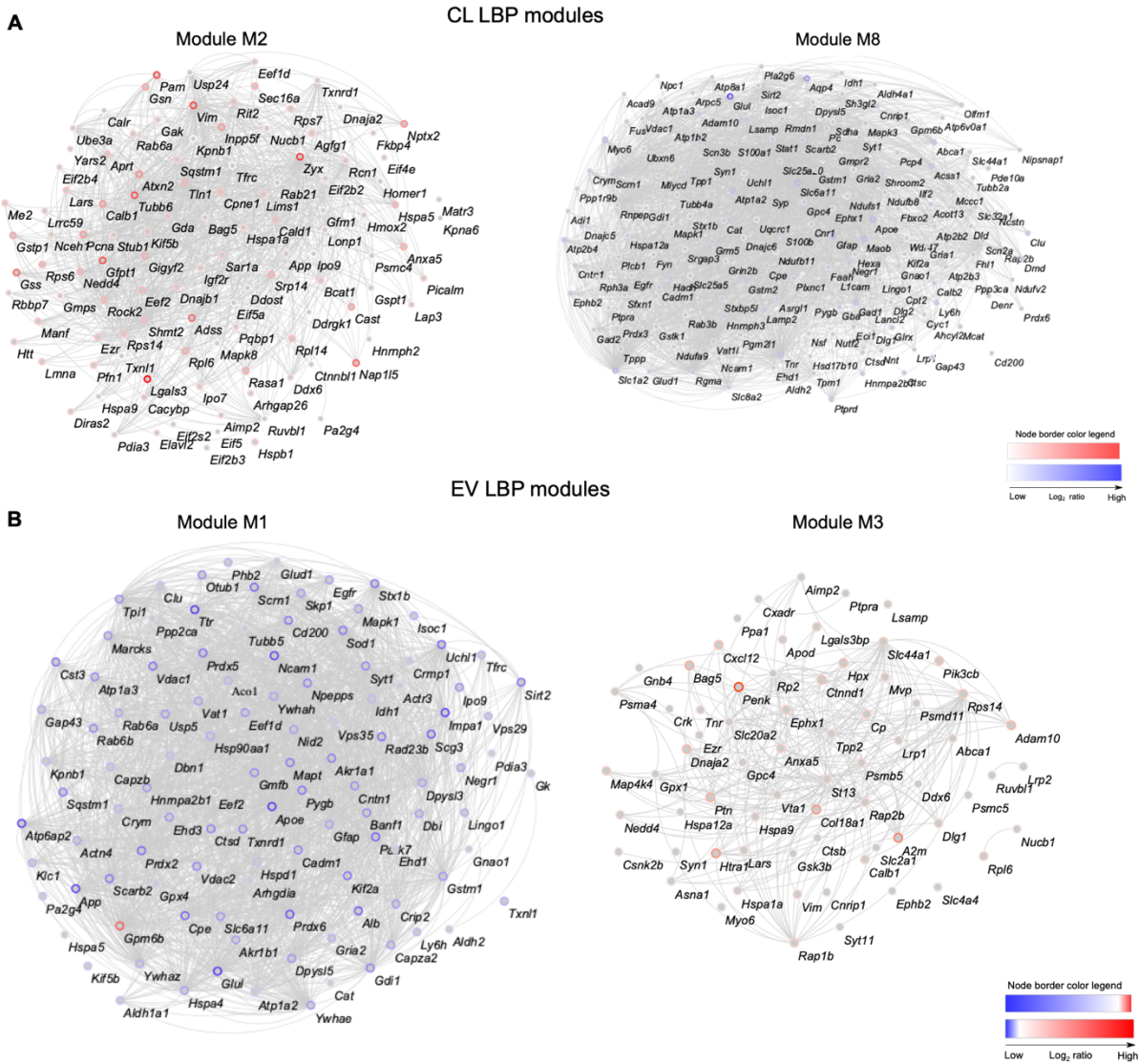
Figure S4. Lewy body pathology (LBP)-enriched Co-expression modules, Related to Figure 3. (**A and B**) The module plots show the Lewy body pathology (LBP) co-expression modules of cell lysate (CL) and extracellular vesicles (EV) datasets. Note: Interactions (edges) represent the correlations between the proteins (labels are gene symbols corresponding to proteins).

Figure S5. Protein-protein interaction network of Alpha-synuclein interacting partners, Related to Figure 4, 5, 6, and Figure S8. (**A**) Schema describing the workflow for generating protein-protein interaction network of alpha-synuclein interacting partners. (**B**) The protein-protein interaction networks in 38 out of 115 proteins were found in STRING DB: 29 common LBP proteins between the cell lysate (CL) and extracellular vesicles (EV) datasets and 9 alpha-synuclein interacting proteins in LBP modules and their 50 interaction neighbors. Nodes are proteins labeled with gene symbols and lines (edges) between the proteins represent the protein interactions.

Contribution of variables via PCA
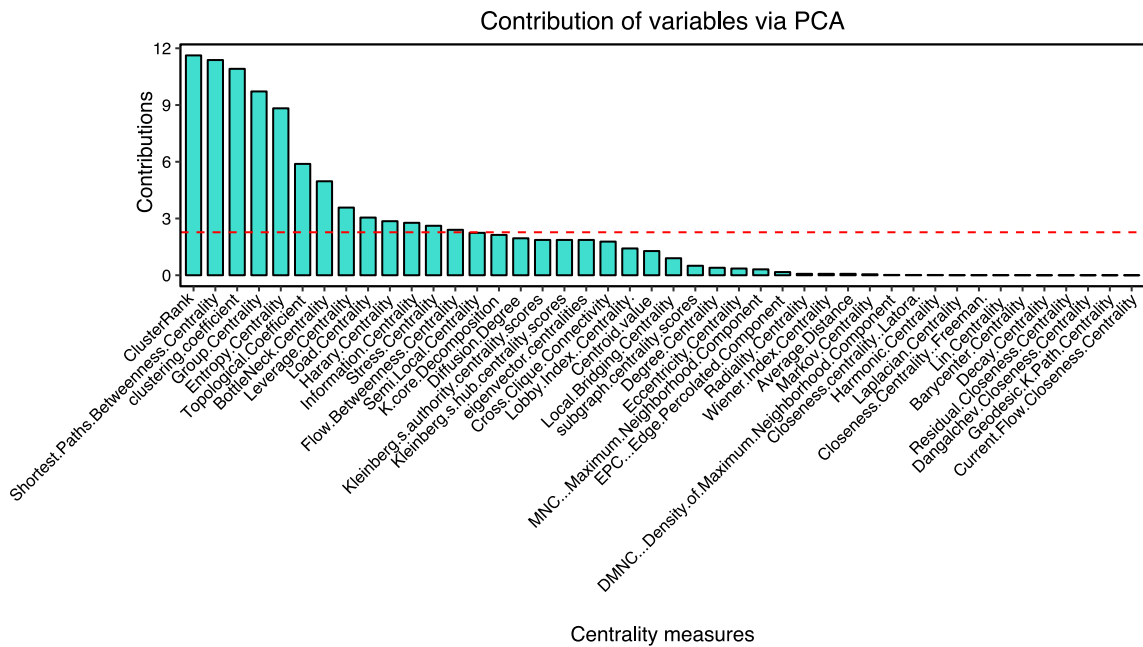
Figure S6. The bar plot demonstrates the centralities measures of a composite module, Related to Figure 5. Red line indicates the random threshold of contribution.
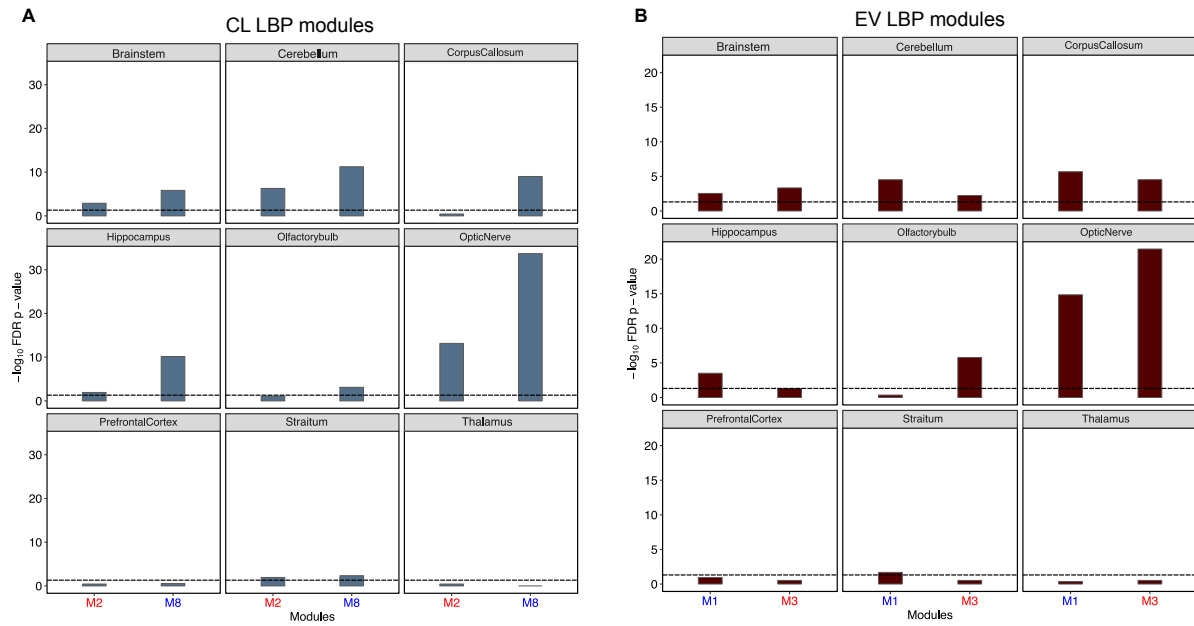
Figure S7. Distribution of cell lysate (CL) and extracellular vesicles (EV) LBP modules in brain regions, Related to Figure 6. (**A and B**) The bar plots show Lewy body pathology (LBP) co-expression modules of CL and EV datasets enrichment in brain regions. Note: The y-axis of bar plot denotes negative $\log_{10}$ Benjamini–Hochberg-adjusted P-values; Fisher's exact test. Note: Red and blue color denotes up and down regulation respectively.
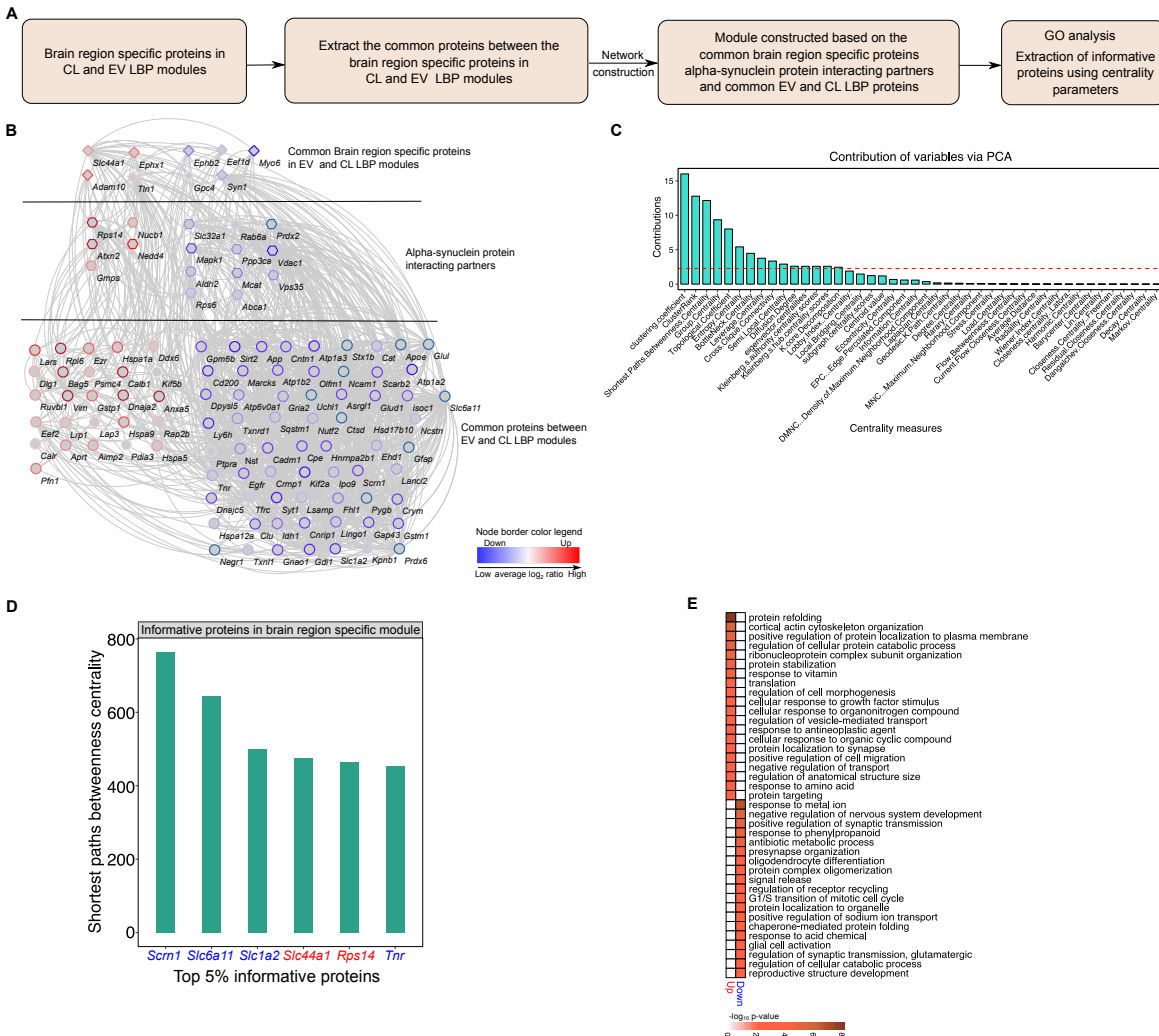
Figure S8. Influence of cell lysate (CL) and extracellular vesicles (EV) LBP modules in Brain regions, Related to Figure 6. (**A**) Schematic representation describing the workflow for common brain region specific module analysis. (**B**) Composite protein interaction module (CPIM) represents common brain region specific protein between the CL and EV pellet common LBP modules alpha-synuclein protein interacting partners and common CL and EV LBP modules. (Note: Nodes are proteins but labeled with gene symbols). (**C**) The bar plot exhibits the centrality measures of a common brain region specific module. (**D**) Top5% of informative proteins from common brain region specific module based on the shortest path betweenness centrality. (**E**) The heatmap represents the statistically significant (negative $\log_{10}$ P-value ≤ 0.05, hypergeometric test from METASCAPE) up and down biological processes GO terms enriched in the common brain region specific protein LBP module. Note: Red and blue color denotes up and down regulation respectively.
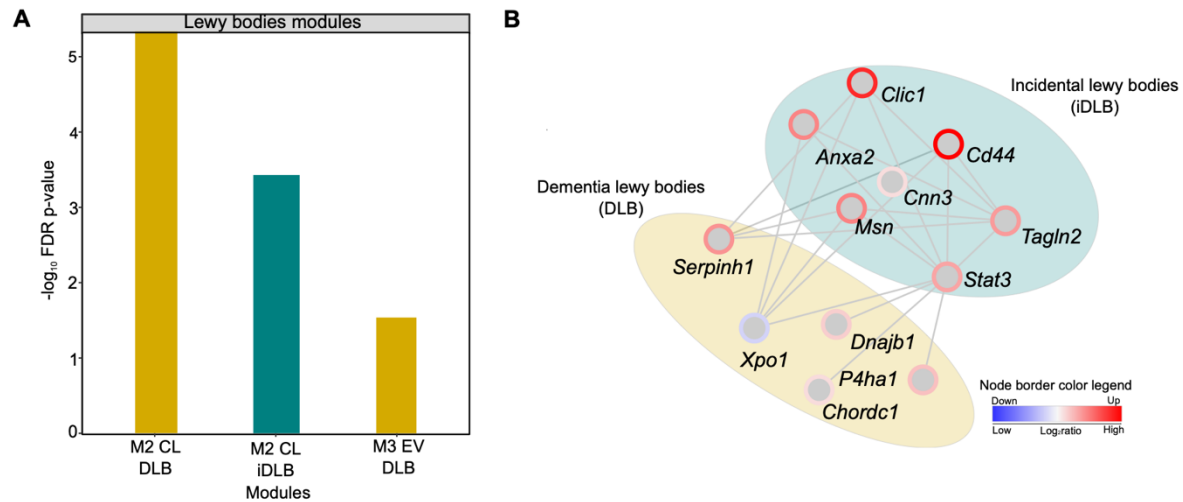
Figure S9. Division of cell lysate (CL) and extracellular vesicles (EV) LBP modules in lewy body related modules, Related to Figure 3. (**A**) The bar plot illustrate LBP co-expression modules of CL and EV datasets enrichment in lewy body disease modules identified by (Santpere et al., 2018) (Note: The y-axis of bar plot denotes negative $\log_{10}$ Benjamini–Hochberg-adjusted P-values; Fisher's exact test). (**B**) The module represents the interactions between the Lewy body related proteins in CL and EV. Note: Red and blue color denotes up and down regulation.

TRANSPARENT METHODS:

Key Resource Table:

Reagent/ Resource/ Software	Source	IDENTIFIER/VERSION
Maxquant software	https://maxquant.net/maxquant/	V 1.6.1.0
Perseus	https://maxquant.net/perseus/	V 1.5.8.5
UniProt database	https://www.uniprot.org	V 2019_10
R software	https://www.r-project.org	V 3.5.1
WGCNA	https://horvath.genetics.ucla.edu/html/ CoexpressionNetwork/Rpackages/WG CNA/	V 1.68
CINNA R package	https://cran.r-project.org/web/package	V 1.1.53
Scatter plot3D R Package	https://cran.r-project.org/web/packages/scatterplot3 d/index.html	V 0.3-41
Factoextra R Package	https://cran.r-project.org/web/packages/factoextra/in dex.html	V 1.0.5
PreprocessCore R package	https://www.bioconductor.org/packag es/release/bioc/html/preprocessCore.ht ml	V 1.44.0
ggplot2 R package	https://cran.r-project.org/web/packages/ggplot2/inde x.html	V 2.3.3
Vennuelar R package	https://cran.r-project.org/web/packages/venneuler/in dex.html	V 1.1-0
Biomart R package	http://bioconductor.org/packages/relea se/bioc/html/biomaRt.html	V 2.38.0
DisGeNet Database	https://www.disgenet.org	V 7.0
Rat Genome Database	https://rgd.mcw.edu/rgdweb/homepag e/	V 20
hRBPome Database	http://caps.ncbs.res.in/hrbpome/	V 1.0
Channelpedia Database	https://channelpedia.epfl.ch	V 1.0
Human protein atlas Database	https://www.proteinatlas.org	V 19.3
STRING Database	https://string-db.org	V 11

Cytoscape	https://cytoscape.org	V 3.7.1
Metascape	https://metascape.org/gp/index.html#/main/step1	V 1.0
Easy nLC 1000	Thermo Scientific	LC 120
Easy nLC 1200	Thermo Scientific	LC 140
Q-Exactive	Thermo Scientific	
Q-Exactive HF	Thermo Scientific	
SP3 digestion	Sielaff, M., et al., Evaluation of FASP, SP3, and iST Protocols for Proteomic Sample Preparation in the Low Microgram Range. J Proteome Res, 2017. 16(11): p. 4060-4072.	
Protein lobind Tubes 0.5 mL	Eppendorf	0030108094
Protein lobind Tubes 1.5 mL	Eppendorf	0030108116
30 cm × 75 µm fused silica emitter	New Objective	FS-360-75-8-N-5-C30
ReproSil-Pur 120 C18-AQ	Dr. Maisch GmbH	r119.aq.0003
Tris	Millipore	648310-M
NaCl	Supelco	1.06404
Triton X-100	Sigma Aldrich	T8787
EDTA	Sigma Aldrich	E9884
Sodium Deoxycholate	Sigma Aldrich	30970
Benzonase	Millipore	E1014
MgCl2	Sigma Aldrich	M3634
Dithiothreitol	Sigma Aldrich	D5545
Iodoacetamide	Sigma Aldrich	I1149
SpeedBeads™ magnetic carboxylate modified particles	GE Healthcare	45152105050250
SpeedBeads™ magnetic carboxylate modified particles	GE Healthcare	65152105050250
LysC	Promega	V1671
Trypsin	Promega	V5111
Ethanol	Supelco	1.11727.2500

H2O + 0.1% formic acid	Biosolve	0023244101BS
Acetonnitrile + 0.1% formic acid	Biosolve	0001934101BS
Acetonitrile	Biosolve	01204101
bFGF	Peprotech	100-18B
anti-GFP	GeneTex	GTX113617
anti-Alix/AIP1	Merck	ABC40
anti-CD81	Santa Cruz Biotechnology	sc-166029
rabbit anti-rat EEA1	Cell Signaling Technology	C8R1
Neurobasal media	Invitrogen	
MLA-80 rotor	Beckmann	
TLA-55 rotor	Beckmann	
SW55Ti rotor	Beckmann	
TLA 110 rotor	Beckmann	
Phosphate buffer saline	Thermo-Fischer-scientific	10010023
RIPA Buffer	Thermo-Fischer-scientific	89900

Hippocampus Primary Neuronal Culture and Sample Preparation:

All experiments were approved by the local animal welfare committee. E18 pregnant rats were purchased from Charles River. Neurons were isolated at embryonic day 18 hippocampus and cultured in Neurobasal Media (2% B27, 0.25% glutamine, 0.125% glutamate (purchased from Invitrogen) (Schwenk et al., 2016) in a NUNC 60 X 15 dish (purchased from Thermo-Scientific). Neurons were treated with 50 ng/ml basic fibroblast growth factor (bFGF) (purchased from Peprotech) to prepare the replicates of bFGF treated condition. Dishes growing neurons were used to collect CL replicates and media from the same neurons was used to isolate EV pellets.

Mass Spectrometry and Data Analysis:

Proteolytic digestion: Neurons were lysed directly on the plate in a modified RIPA lysis buffer (50 mM TrisHCl pH 8, 150 mM NaCl, 5 mM EDTA, 1% (v/v) Triton X-100, 0.5% (w/v) sodium deoxycholate, 0.1% (w/v) with protease inhibitors (Sigma Aldrich, US) on ice using a cell scraper to prepare CL samples. An amount of 20 μg of protein according to a BCA protein assay was used for further sample preparation. EV pellets were lysed by using 80 μL of the modified RIPA lysis buffer on ice with intermediate vortexing. Both cell lysates and EV samples were diluted 1:2 with water and 100 mM MgCl2 was added to a final concentration of 10 mM. Afterwards, 25 units Benzonase (Sigma Aldrich, US) were added and samples were incubated for 30 min at 37°C at 1400 rpm in a Thermomixer (Eppendorf, Germany). Undissolved material was removed via centrifuging them for 5 min at 20,000 g and 4°C and supernatants were then transferred to fresh Eppendorf tubes. Proteins were reduced by addition of 9 μL of 200 mM dithiothreitol (Biozol, Germany) in 50 mM ammonium bicarbonate incubated at 37°C for 30 min. Alkylation of cysteine residues was achieved by adding 18 μL 400 mM iodoacetamide (Sigma Aldrich, US) and 30 min incubation in the dark at room temperature. Afterwards, reaction was quenched by adding another 9 μL of 200 mM dithiothreitol. Proteolytic digestion was performed using a modified protocol for single-pot solid-phase enhanced sample preparation (SP3) (Sielaff et al., 2017).

LC-MS/MS analysis

Peptides from digestion of CL and EV samples were analyzed on an Easy nLC 1200 coupled to a Q-Exactive HF mass spectrometer and an Easy nLC 1000 nanoHPLC coupled to a Q-Exactive mass spectrometer (Thermo Scientific, US). Both systems were equipped with a PRSO-V1 column oven (Sonation, Germany). 1 μg peptides per sample were separated on custom packed

C18 columns (30 cm x 75 µm ID, ReproSil-Pur 120 C18-AQ, 1.9 µm, Dr. Maisch GmbH,Germany) using a binary gradient of water (A) and acetonitrile (B) supplemented with 0.1% formic acid (Gradient for CL: 0 min., 2.4% B; 2 min., 4.8% B; 92 min., 24% B; 112 min., 35.2% B; 121 min., 60% B; Gradient for EV: 0 min., 2% B; 3:30 min., 5% B; 137:30 min., 25% B; 168:30 min., 35% B; 182:30 min., 60% B) at 50°C column temperature. Full MS scans were acquired at the resolution of 120,000 for CL and 70,000 for EV (m/z range: 300-1400, AGC target: 3E+6). For CL the top 15 peptide ions were chosen for Higher-energy C-trap Dissociation (HCD) (resolution: 15,000, isolation width: 1.6 m/z, AGC target: 1E+5, NCE: 26%). For EV samples, the 10 most intense peptide ions per full MS scan were selected for fragmentation (resolution: 17,000, isolation width: 2 m/z, AGC target: 1E+5, NCE: 25%). A dynamic exclusion of 120s was applied.

Maxquant (maxquant.org, Max-Planck Institute Munich) version 1.6.1.0 (Cox et al., 2014) was used to analyze raw data. MS data was searched against an established fasta database of *Rattus norvegicus* on UniProt (download: March 5th 2018, 29975 entries) defining trypsin as protease. For the database search two missed cleavages were allowed. First search option was used to recalibrate the peptide masses within a window of 20 ppm. For main search, peptide and peptide fragment mass tolerances were respectively set to 4.5 and 20 ppm. Carbamidomethylation of cysteine was demarcated as static modification. Acetylation of the protein N-term and oxidation of methionine were set as variable modifications. Hippocampal neurons were cultured from 3 different rats and 8 repeats (dishes) were prepared for the collection of EVs and CL. Mass spectrometry has been performed with the following number of (n) replicates: Extracellular vesicles (EV): bFGF (n = 7); Vehicle (n = 6). Cell lysate (CL): bFGF (n = 8); Vehicle (n = 8). False discovery rate for both peptides and proteins were adjusted to less than 1%. Label free quantification (LFQ) of proteins required at least two ratio counts of razor peptides. Only razor and unique peptides were used for quantification. Protein LFQ intensities were log2 transformed and significance of protein changes was evaluated by two-sided Student's t-test. Additionally, a permutation n-based false discovery rate (FDR) estimation was used. The significantly changed proteins were identified using FDR.

Weighted Protein Co-Expression Network (WPCNA) Analysis of Cell Lysate and Exosome Proteome:

We first performed quantile normalization of the $\log_2$ transformed values to build the proteome-wide co-expression networks from CL and EV datasets. This normalized data was taken further to weighted co-expression gene network analysis using the WGCNA R package (Langfelder and Horvath, 2008) and constructed the modules from each dataset separately. As we used proteome data, we refer network analysis method as WPCNA works as follows: 1) computes Pearson correlations for all protein-protein pairs and converts into an adjacency matrix by taking their absolute value and raising it to the power function. 2) This function transforms adjacencies into a topological overlap matrix (TOM). Proteins were clustered using average linkage hierarchical clustering. The following parameters were used to build co-expression modules: Softpower: 3, dynamic deep split: 4, minimum module size 30 and merge height: 0.04. To evaluate statistical significance of the co-expression modules, module quality statistics was calculated by re-sampling the networks using the *module Preservation* function in the WGCNA R package. We arbitrarily permutated the protein labels 500 times and computed the Z-scores (Z-Summary) for module quality statistics such as module membership and connectivity. Z-Summary >10 was used to identify the significant gene co-expression modules in comparison to random module (Langfelder et al., 2011)**.** Module membership was calculated for each protein as a Module Eigenprotein (ME) and described as first principal component assists as an expression profile of module. We measured the relative number of common proteins between the co-expression modules using the Jaccard similarity co-efficient (J).

Extraction of LBP Co-Expression Modules:

To determine if any Parkinson's disease (PD) associated targets relevant for Lewy Body Pathology (LBP) are enriched in modules, we used PD-proteome screens from publications (Boerger et al., 2019, Dumitriu et al., 2015, Lachén-Montes et al., 2019). Additionally, we extracted PD linked genes from following resources: DisGeNET (www.disgenet.org), Rat Genome Database (RGD) (rgd.mcw.edu) and GWAS studies (Klemann et al., 2017) .We collected PD gene lists from all the sources as discussed above and converted their Gene symbols (GS) to rat genes using the Biomart R package. These rat genes were used to assess PD enrichment by cross-referencing CL and EV proteome modules via matching gene symbols.

LBP Module Enrichment Analysis:

We performed LBP modules enrichment with variety of resources as follows: 1) we took human RNA binding proteins (RBPs) from hRBPome database to identify RBPs and their interactions (http://caps.ncbs.res.in/hrbpome/). 2) Alpha- synuclein protein partners were extracted from Khurana V et.al (Humanized networks) (Khurana et al., 2017). 3) We mined following receptors and channels from (https://www.proteinatlas.org/) and Channelpedia (https://channelpedia.net/). *Ionotropic receptors*: GABAA receptors, Glutamate NMDA receptors, Glutamate Kainate receptors, Glutamate AMPA receptors, Glycine receptors, Nicotinic Acetylcholine receptors, and Serotonin 5-HT3 receptor. *Metabotropic receptors*: Adrenergic receptors, Dopamine receptors, GBAB receptors, Glutamate receptors mGluR, Histamine receptors, Muscarinic acetylcholine receptors (mAChR), Opioid receptors, and serotonin (5-HT) receptors. *Ion channel proteins*: Potassium (K), Sodium (Na), Calcium (Ca), Chloride (Cl), Hyperpolaraization-activated channel (Ih),Tranient receptor potential channels (TRP). 4) We extracted the cellular localization of RNA binding proteins from https://www.proteinatlas.org/humanproteome/cell/organelle 5) The list of proteins related to different regions of brain such as Hippocampus, Striatum, Thalamus, Cerebellum, Brain stem, Olfactory bulb, Motor cortex, Prefrontal cortex, Corpus callosum, and Optic nerve were downloaded from mouse brain proteome (Sharma et al., 2015). 6) We retrieved Lewy body-related hub genes from previously published frontal cortex human transcriptome dataset (Santpere et al., 2018). Gene symbols (GS) from all the datasets discussed above were converted to rat genes using the Biomart R package and intersected with LBP modules.

Construction of Common Alpha-Synuclein Composite Brain Region-specific LBP Modules:

The common LBP proteins between the CL, EV and alpha-synuclein protein interaction partners were used to construct the protein-protein interaction module using STRING database (Szklarczyk et al., 2019). We mapped interactions amongst the receptors, channels, RNA-binding proteins, common alpha-synuclein protein interaction partners of cell lysate and exosome LBP modules to build the composite module. To construct the brain region specific module, we retrieved the interactions between the common brain region specific proteins, alpha-synuclein protein interacting partners in cell lysate and exosome LBP modules.

Key proteins identification and connectivity analysis in co-expression modules:

We identified interconnected proteins with in the common module (High Jaccard index) by module connectivity, measured by absolute value of Pearson correlation (cor.proteinModuleMembership) MM >0.9 function from WGCNA R package (Langfelder and Horvath, 2008). Furthermore, we uploaded proteins with MM>0.9 to STRING database and constructed protein-protein interactions and degree ≥ 7 were considered as highly connected proteins in the shared module between cell lysate and exosome. To extract the most informative proteins in composite and common brain region specific LBP modules we evaluated centrality parameters using CINNA R package (Ashtiani et al., 2019) this method was also used to find most suitable centrality parameter based on which we mined the central proteins from the modules. We computed Connectivity Score (CS) a measure of connectedness for the module by summing up the weight scores generated by WGCNA (Burkett et al., 2018).

Pathway Enrichment Analysis:

The pathway enrichment of co-expression modules was examined with METASCAPE (www.metascape.org) using biological process (BP) annotations which were obtained from gene ontology (GO). We considered BP as statistically significant using a p-value ≤ 0.05 (the p-values are expressed as $\log_{10}$, i.e., -2 represents 0.01 p-value).

Statistical Evaluation and Data Visualization:

The statistical evaluation and visualization if not stated otherwise, was performed using the R statistical environment v3.5.1 (https://www.r-project.org/). Pearson correlation analyses between the replicates was calculated and visualized as a heatmap using corrplot package in R. Unsupervised clustering of proteome data was performed using the Principal component analysis (PCA) in R and three-dimensional PCA was visualized using scatterplot3D R package. A hierarchical cluster analysis of proteome data was executed using the average linkage clustering and Euclidean similarity metric in R, clustered dendrogram was visualized using the factoextra R package. Quantile normalization of proteome datasets was performed using the preprocessCore R package. Boxplot analysis of the module eigenprotein of co-expression modules was performed using the ggplot2 R package and statistical significance was evaluated using Wilcoxon-test. The Jaccard similarity co-efficient (J)$J = |M_d \cap M_e| \, / \, |M_d \cup M_e|$, whereas M_d and M_e are proteins in modules. Statistical assessment of LBP module enrichment was done using the Fisher's exact test

and adjusted for multiple comparisons by the FDR (P ≤ 0.05) Benjamini-Hochberg (BH) method and converted p-values to negative $\log_{10}$. Bar plots were visualized using the ggplot2 R package. All the module plots were pictured in Cytoscape v3.7.1 (www.cytoscape.org). Venn diagram and the heatmaps were generated using the venneuler and pheatmap R packages respectively.

REFERENCES:

ASHTIANI, M., MIRZAIE, M. & JAFARI, M. 2019. CINNA: an R/CRAN package to decipher Central Informative Nodes in Network Analysis. *Bioinformatics,* 35**,** 1436-1437.

BOERGER, M., FUNKE, S., LEHA, A., ROSER, A.-E., WUESTEMANN, A.-K., MAASS, F., BÄHR, M., GRUS, F. & LINGOR, P. 2019. Proteomic analysis of tear fluid reveals disease-specific patterns in patients with Parkinson's disease – A pilot study. *Parkinsonism & Related Disorders,* 63**,** 3-9.

BURKETT, Z. D., DAY, N. F., KIMBALL, T. H., AAMODT, C. M., HESTON, J. B., HILLIARD, A. T., XIAO, X. & WHITE, S. A. 2018. FoxP2 isoforms delineate spatiotemporal transcriptional networks for vocal learning in the zebra finch. *eLife,* 7.

COX, J., HEIN, M. Y., LUBER, C. A., PARON, I., NAGARAJ, N. & MANN, M. 2014. Accurate proteome-wide label-free quantification by delayed normalization and maximal peptide ratio extraction, termed MaxLFQ. *Mol Cell Proteomics,* 13**,** 2513-26.

DUMITRIU, A., GOLJI, J., LABADORF, A. T., GAO, B., BEACH, T. G., MYERS, R. H., LONGO, K. A. & LATOURELLE, J. C. 2015. Integrative analyses of proteomics and RNA transcriptomics implicate mitochondrial processes, protein folding pathways and GWAS loci in Parkinson disease. *BMC Medical Genomics,* 9**,** 5-5.

KHURANA, V., PENG, J., CHUNG, C. Y., AULUCK, P. K., FANNING, S., TARDIFF, D. F., BARTELS, T., KOEVA, M., EICHHORN, S. W., BENYAMINI, H., LOU, Y., NUTTER-UPHAM, A., BARU, V., FREYZON, Y., TUNCBAG, N., COSTANZO, M., SAN LUIS, B. J., SCHONDORF, D. C., BARRASA, M. I., EHSANI, S., SANJANA, N., ZHONG, Q., GASSER, T., BARTEL, D. P., VIDAL, M., DELEIDI, M., BOONE, C., FRAENKEL, E., BERGER, B. & LINDQUIST, S. 2017. Genome-Scale Networks Link Neurodegenerative Disease Genes to alpha-Synuclein through Specific Molecular Pathways. *Cell Syst,* 4**,** 157-170 e14.

KLEMANN, C. J. H. M., MARTENS, G. J. M., SHARMA, M., MARTENS, M. B., ISACSON, O., GASSER, T., VISSER, J. E. & POELMANS, G. 2017. Integrated molecular landscape of Parkinson's disease. *npj Parkinson's Disease,* 3**,** 14-14.

LACHÉN-MONTES, M., GONZÁLEZ-MORALES, A., ILORO, I., ELORTZA, F., FERRER, I., GVERIC, D., FERNÁNDEZ-IRIGOYEN, J. & SANTAMARÍA, E. 2019. Unveiling the olfactory proteostatic disarrangement in Parkinson's disease by proteome-wide profiling. *Neurobiology of Aging,* 73**,** 123-134.

LANGFELDER, P. & HORVATH, S. 2008. WGCNA: an R package for weighted correlation network analysis. *BMC Bioinformatics,* 9**,** 559-559.

LANGFELDER, P., LUO, R., OLDHAM, M. C. & HORVATH, S. 2011. Is My Network Module Preserved and Reproducible? *PLoS Computational Biology,* 7**,** e1001057-e1001057.

SANTPERE, G., GARCIA-ESPARCIA, P., ANDRES-BENITO, P., LORENTE-GALDOS, B., NAVARRO, A. & FERRER, I. 2018. Transcriptional network analysis in frontal cortex in Lewy body diseases with focus on dementia with Lewy bodies. *Brain Pathology,* 28**,** 315-333.

SCHWENK, B. M., HARTMANN, H., SERDAROGLU, A., SCHLUDI, M. H., HORNBURG, D., MEISSNER, F., OROZCO, D., COLOMBO, A., TAHIROVIC, S., MICHAELSEN, M., SCHREIBER, F., HAUPT, S., PEITZ, M., BRÜSTLE, O., KÜPPER, C., KLOPSTOCK, T., OTTO, M., LUDOLPH, A. C., ARZBERGER, T., KUHN, P.-H. & EDBAUER, D. 2016. TDP-43 loss of function inhibits endosomal trafficking and alters trophic signaling in neurons. *The EMBO Journal,* 35**,** 2350-2370.

SHARMA, K., SCHMITT, S., BERGNER, C. G., TYANOVA, S., KANNAIYAN, N., MANRIQUE-HOYOS, N., KONGI, K., CANTUTI, L., HANISCH, U. K., PHILIPS, M. A., ROSSNER, M. J., MANN, M. & SIMONS, M. 2015. Cell type- and brain region-resolved mouse brain proteome. *Nat Neurosci,* 18**,** 1819-31.

SIELAFF, M., KUHAREV, J., BOHN, T., HAHLBROCK, J., BOPP, T., TENZER, S. & DISTLER, U. 2017. Evaluation of FASP, SP3, and iST Protocols for Proteomic Sample Preparation in the Low Microgram Range. *J Proteome Res,* 16**,** 4060-4072.

SZKLARCZYK, D., GABLE, A. L., LYON, D., JUNGE, A., WYDER, S., HUERTA-CEPAS, J., SIMONOVIC, M., DONCHEVA, N. T., MORRIS, J. H., BORK, P., JENSEN, L. J. & MERING, C. V. 2019. STRING v11: protein–protein association networks with increased coverage, supporting functional discovery in genome-wide experimental datasets. *Nucleic Acids Research,* 47**,** D607-D613.